energies

MDPI

Review

A Comprehensive Review and Analytical Comparison of Non-Isolated DC-DC Converters for Fuel Cell Applications

Furqan A. Abbas [1,†], Thealfaqar A. Abdul-Jabbar [1,†], Adel A. Obed [1], Anton Kersten [2,*], Manuel Kuder [2] and Thomas Weyh [2]

[1] Department of Electrical Power Engineering, Middle Technical University, Baghdad 10011, Iraq
[2] Department of Electrical Engineering, Bundeswehr University Munich, 85577 Neubiberg, Germany
* Correspondence: anton.kersten@unibw.de
† These authors contributed equally to this work.

Abstract: The use of renewable energy sources such as solar photovoltaic, wind, and fuel cells is becoming increasingly prevalent due to a combination of environmental concerns and technological advancements, as well as decreasing production costs. Power electronics DC-DC converters play a key role in various applications, including hybrid energy systems, hybrid vehicles, aerospace, satellite systems, and portable electronic devices. These converters are used to convert power from renewable sources to meet the demands of the load, improving the dynamic and steady-state performance of green generation systems. This study presents a comparison of the most commonly used non-isolated DC-DC converters for fuel cell applications. The important factors considered in the comparison include voltage gain ratio, voltage switch stress, voltage ripple, efficiency, cost, and ease of implementation. Based on the comparison results, the converters have been grouped according to voltage level applications, with low voltage applications being best served by converters such as DBC, DuBC, TLBC, 2-IBC, 1st M-IBC, PSOL, SEPIC, and 1st M-SEPIC owing to their lower cost, smaller size, and reduced switch stress. Medium voltage applications are best suited to converters such as TBC, 1st M-TLBC, 2nd M-TLBC, 4-IBC, 1st M-IBC, 2nd M-IBC, 1st M-PSOL, 2nd M-PSOL, 1st M-SEPIC, and 2nd M-SEPIC, which offer higher efficiency. Finally, high voltage applications are best served by converters such as TBC, 1st M-TBC, 2nd M-IBC, 3rd M-IBC, 3rd M-PSOL, 4th M-PSOL, 2nd M-SEPIC, 3rd M-SEPIC, and 4th M-SEPIC.

Keywords: analytical comparison; DC-DC converters; energy conversion; fuel cell applications; fuel cell systems; non-isolated converters; power management; power converter applications

Citation: Abbas, F.A.; Abdul-Jabbar, T.A.; Obed, A.A.; Kersten, A.; Kuder, M.; Weyh, T. A Comprehensive Review and Analytical Comparison of Non-Isolated DC-DC Converters for Fuel Cell Applications. *Energies* **2023**, *16*, 3493. https://doi.org/10.3390/en16083493

Academic Editor: Carlos Quiterio Gómez Muñoz

Received: 15 February 2023
Revised: 28 March 2023
Accepted: 12 April 2023
Published: 17 April 2023

1. Introduction

Most power is generated from traditional energy sources, such as coal, petroleum, or natural gas, which emit carbon dioxide and contribute to global warming. The primary cause of climate change is the burning of fossil fuels, which releases greenhouse gases (GHG) into the atmosphere. Nearly 80 % of GHGs are generated by the use of fossil fuels. However, the world's primary energy demand is projected to grow by nearly 60 % between 2002 and 2030, with an average annual increase of 1.7 %, leading to further GHG emissions. It is projected that oil reserves will be exhausted by 2040, natural gas by 2060, and coal by 2300 [1]. Given this reality, there is a growing need to develop renewable energy sources (RES) as a means to produce clean and emission-free energy. The search for RES has become an urgent issue [2,3].

RES such as wind power, fuel cells (FC), and photovoltaic (PV) are increasingly being used in various applications, including motor drives, uninterruptible power systems, electric vehicles, microgrids, and more. As presented in [3,4], green hydrogen can play a vital role in reducing the carbon footprint, ensuring sustainability in the transportation and energy sector. Therefore, FCs are one of the key players in the global energy sector, as they

are electrochemical devices that convert chemical reactions into electrical energy through an electrolytic process, producing only heat and water as byproducts. There are several types of FCs, including alkaline FCs, phosphoric FCs, molten carbonate FCs, solid oxide FCs, combined heat and power FCs, proton exchange membrane FCs, and regenerative and reversible FCs, each with unique characteristics based on the nature of their application [5]. The most widely used FC type is the proton exchange membrane fuel cell (PEMFC) due to its better efficiency, zero or low emissions, low noise level, and lower operating temperature. However, PEMFC systems have a slow output power and an unregulated DC voltage due to the complex mechanical design and the electrochemical nature of its polarization curve. Variations in operating conditions such as pressure, temperature, mass flow rate, relative humidity, water content, air, hydrogen stoichiometry, and channel shape can impact the electrochemical reaction and thus affect the voltage generated by the FC, requiring the connection of power converters to the load [6].

Power electronic converters serve as intermediaries between power generation and load, primarily used to regulate the input voltage according to the application requirements. For decades, power converters have been prevalent in power engineering and drives and have been adopted to replace conventional voltage divider circuits, including rheostats and power conversion circuits [7]. These conventional methods typically have low output voltage and efficiency. DC-DC converters were first proposed in the 1920s and have been widely used in various applications for over six decades, playing a crucial role in power electronics and drives. They are utilized in many industrial applications, computer hardware circuits, and especially in renewable energy generation. Converters are a critical component of any hybrid renewable energy system as they can stabilize the voltage output during intermittent conditions. The power quality of renewable energy systems heavily depends on the stable operation and control technique of the power converter [8,9]. The first boost converters were used, and then various techniques were derived from conventional boost converters to improve efficiency and conversion rate. These new converter versions aimed to achieve a high voltage gain ratio, increased efficiency, reduced voltage stress, and reduced ripple [10,11].

This paper designs and analyzes the most common types of non-isolated converters, which consist of Multilevel Boost Converters (MLBC) [12–16], Three-Level Boost Converters (TLBC) [17–19], Interleaved Boost Converter (IBC) [20–25], Positive Output Super-Lift (POSL) [26–30], Single-Ended Primary Inductor Converter (SEPIC) [31–36]. For an FC to maximize its output voltage, it is important to investigate the key performance of these converters in terms of voltage gain ratio and voltage stress.

This paper is organized as follows: Section 2 discusses the FC model, and the types of DC-DC converters are discussed in Section 3. The simulation result and comparison between the converters are described in Section 4. Finally, concluding remarks are provided in Section 5.

2. Fuel Cell (FC) Model

The FC operates similarly to a battery with an anode and a cathode, producing a DC voltage. The output voltage of the FC exhibits a noticeable degree of regulation with increasing current, as shown in Figure 1a, where the voltage–current characteristics of a single cell are displayed, with the cell voltage dropping as the current density increases [37,38]. This is due to three types of losses: activation losses, ohmic losses, and concentration losses. Slowness in the chemical reactions at the electrode surfaces causes activation losses, while ohmic losses arise from the contribution of the membrane, electrode material, and various interconnections. Since the voltage drop is related to the current density, operating the FC in the ohmic loss region is advised. The FC can be represented in this region as a Thevenin equivalent circuit consisting of a constant DC voltage source (V_{FC}) and a series resistance (R_{FC}), as illustrated in Figure 1b. Therefore, the actual cell voltage as described in [39], can be expressed as

$$V_{FC} = \Delta V_{ohmic} - \Delta V_{conc} - \Delta V_{activ} \quad (1)$$

where ΔV_{ohmic}, ΔV_{conc}, and ΔV_{activ} are the voltage drop due to the ohmic, concentration, and activation losses, respectively. A membrane separates the two electrodes of the PEMFC, preventing electron flow and allowing only positive ions to pass. The electrons flow from the anode to the cathode's surface via the external circuit, where they recombine with the positive ions, H^+. As a result, opposite-polarity charged layers emerge on the cathode and electrolyte sides of the membrane where the cathode–membrane interface functions as a massive capacitor that stores an electrical charge and energy [40], which is referred to as "double-layer". Figure 2 illustrates the fuel cell parameters that have been presented in this paper.

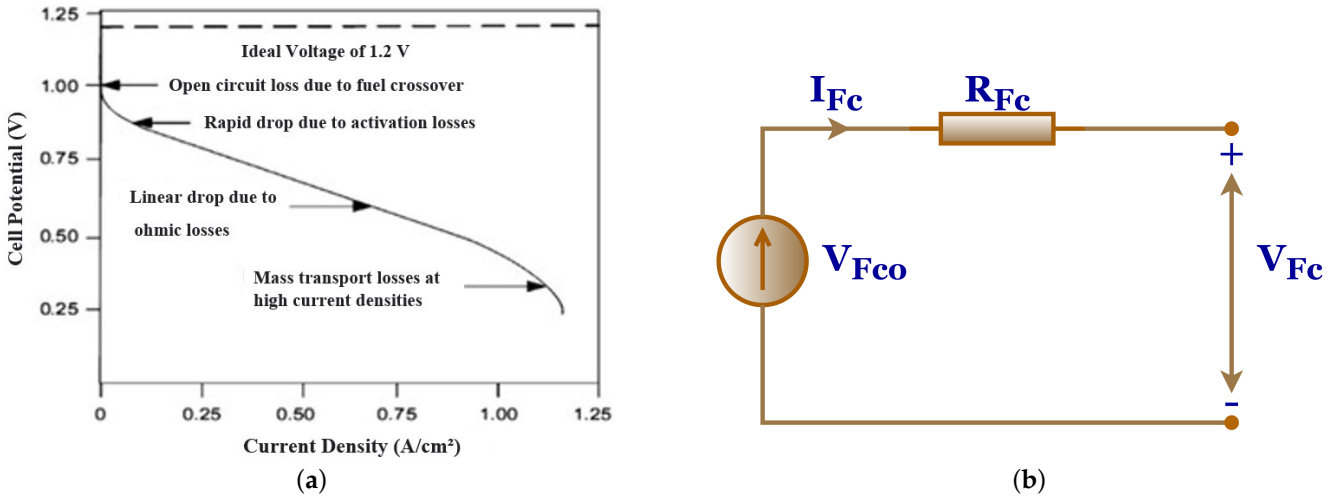

Figure 1. (**a**) *V*–*I* characteristic feature and corresponding (**b**) equivalent circuit model of an FC system.

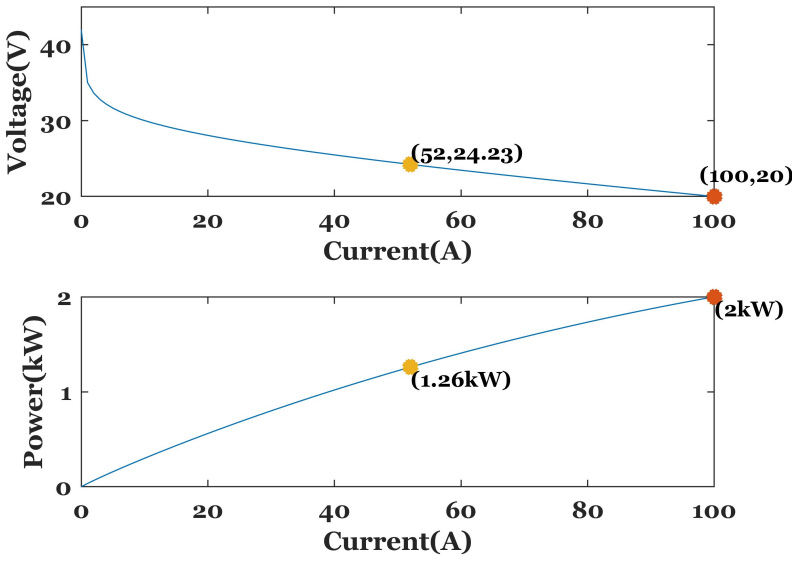

Figure 2. FC stack parameters.

3. DC-DC Converters

The selection of a DC-DC converter is crucial in maximizing the system's output voltage or power and ensuring its overall operating performance. Different DC-DC converter topologies regulate the input voltage to suit the requirements of the corresponding voltage application. There are two main types of DC-DC converters: isolated and non-isolated [41]. Figure 3 illustrates the power converter family and showcases the common converter topologies in both categories [8]. The design of isolated DC-DC converters commonly

features a high-frequency transformer between the input and output, providing galvanic isolation to enhance safety and protect sensitive loads [42]. The output can have either a positive or negative polarity and is highly immune to noise interference. In contrast, non-isolated DC-DC converters do not have galvanic isolation, making them simpler in design and more cost-effective. Due to the presence of a magnetic transformer, isolated DC-DC converters are more suitable for applications that request a high voltage gain ratio. Another characteristic of isolated DC-DC converters is galvanic isolation. However, magnetic transform leads to poor compactness, higher weight, and more complex design [43]. Significant research has been carried out on non-isolated converters, leading to the development of various DC-DC converter topologies for enhanced efficiency, improved switching and control strategies, fault-tolerant operation, and renewable-energy-based applications [44].

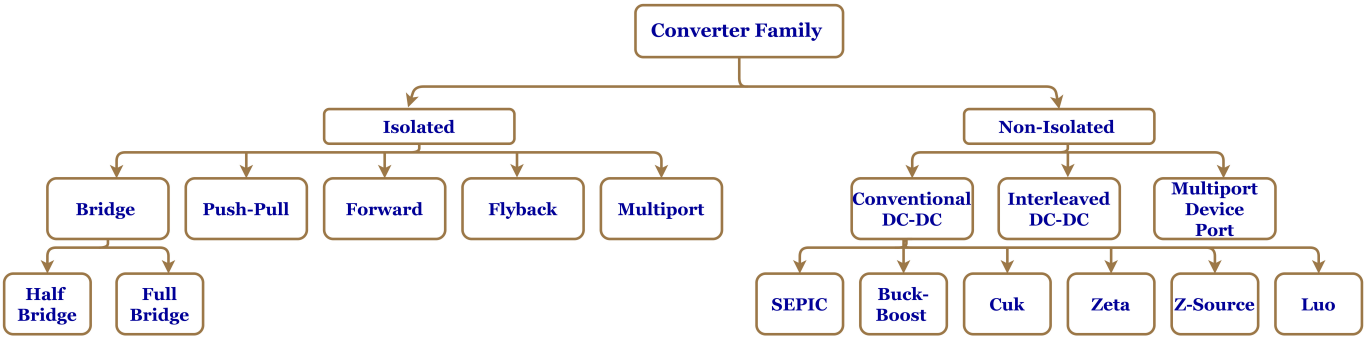

Figure 3. Boostconverter family, including isolated and non-isolated topologies.

Conventional boost converters are widely used in renewable energy applications because of their simple circuit design. In theory, the voltage gain of a boost converter can approach infinity (neglecting ohmic losses) when the duty cycle, is close to unity. However, as the duty cycle increases, the switch's turn-off period becomes shorter, leading to significant current ripples in the power devices. This results in increased conduction losses and turn-off current, and high-voltage stresses in both the switch and diode equal to the output voltage, especially in high-output applications. This can make the cost of high-voltage stress switches relatively higher than those with low-voltage stress. Furthermore, the hard-switching operation of the boost converter causes significant switching and reverse-recovery losses [2]. To address these limitations, several new step-up converter structures have been proposed, and this study compares the most commonly used DC-DC converters.

3.1. Multilevel Boost Converter

The multilevel boost converter (MBC) has been proposed as an improvement over conventional boost converters. This topology integrates the boost converter with a switched capacitor function, providing several benefits such as maximizing the output voltage with the same input voltage and ensuring self-balanced voltage without significantly increasing the complexity of the converter [12,13]. The number of levels in the MBC can be increased by adding capacitors and diodes, enabling modular implementation without changing the converter structure. The MBC comprises only one actively controlled switch, one inductor, $2N$-1 diodes, and $2N$-1 capacitors for an N-level configuration, making it a compact and efficient solution for various power conversion applications.

3.1.1. Dual-Level Boost Converter (DBC)

Figure 4 depicts the dual-level boost converter (DBC) utilized in this study, comprising one actively controlled switch, one inductor, three diodes, and three capacitors. The operation of the DBC is divided into two discrete states [14].

1. During the ON state of switch S, the inductor is connected to V_{in} for charge condition; if C_1's voltage is smaller than C_2's voltage then C_2 clamps C_1's voltage through D_2 and S. At the same time, the voltage across C_3 is still constant, as shown in Figure 4a.
2. Figure 4b illustrates the circuit behavior when the switch, S, is turned OFF, the inductor current flows through D_1 when it is forward biased to charge C_2. When D_1 is still forward biased, the capacitor C_1 and the voltage V_{in} plus the inductor's voltage clamps the voltage across C_3 and C_2 through D_3.

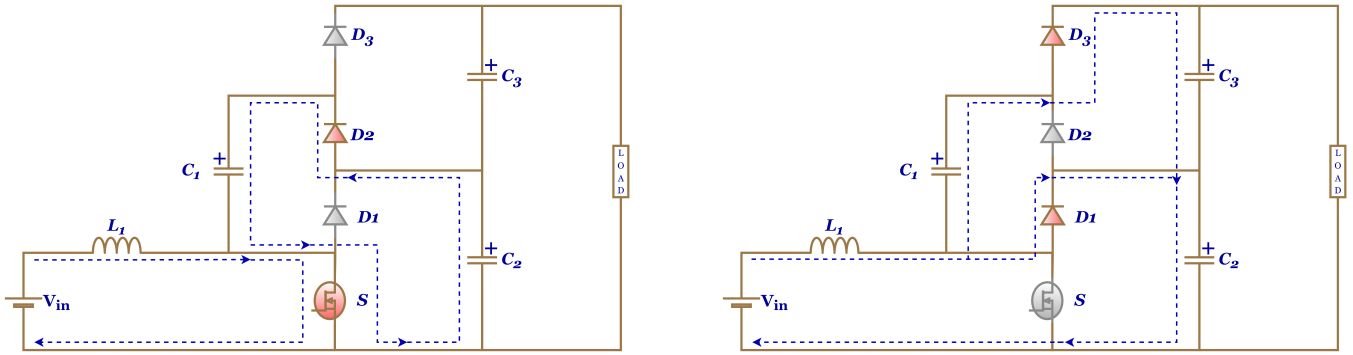

Figure 4. DBC operation: (**a**) S closed and (**b**) S open.

The inductor and capacitors selection values depend on the equations that are listed in Table 1. It can be assumed that capacitors C_1, C_2, and C_3 are equal.

3.1.2. Triple-Level Boost Converter (TBC)

As mentioned earlier, MBC topology makes it easier to accomplish higher voltage gain relays by adding capacitors and diodes where the number of these components is expressed as $2N$-1 diodes and $2N$-1 capacitors to achieve an N level of MBC. This study suggested a Triple-level boost converter (TBC) to reach high-voltage gain and reduce switch stress. The operation of TBC is divided into two states, as shown in Figure 5 [15].

1. The inductor is connected to the input voltage when switch S is closed. If the voltage across C_1 is smaller than C_2, C_1 charges from C_2 through D_2, which operates in forward bias. At the same time, the voltage across $C_1 + C_3$ equals the voltage across $C_2 + C_4$, C_2 and C_4 act as a voltage source to charge C_1 and C_3 through the diode D_4, as indicated in Figure 5a.
2. When the switch S is open, the diode D_1 operates in forward bias allowing the energy stored in the inductor to start charging capacitor C_2. Furthermore, D_3 operates in forward bias, the input voltage, the inductor, and capacitor C_1 supply the capacitors C_2 and C_4. When the voltage on $C_2 + C_4$ is equal to the total voltage on the input voltage, the inductor voltage, and the capacitor voltage C_1 through D_5 operates in forward bias, the input voltage, inductor, and capacitors C_1 and C_3 charge capacitors C_2, C_4 and C_5 as demonstrated in Figure 5b.

The selection values of the inductor and capacitors depend on equations that are illustrated in Table 1 for calculating TBC parameters. It is assumed capacitors C_1, C_2, C_3, C_4 and C_5 are equal.

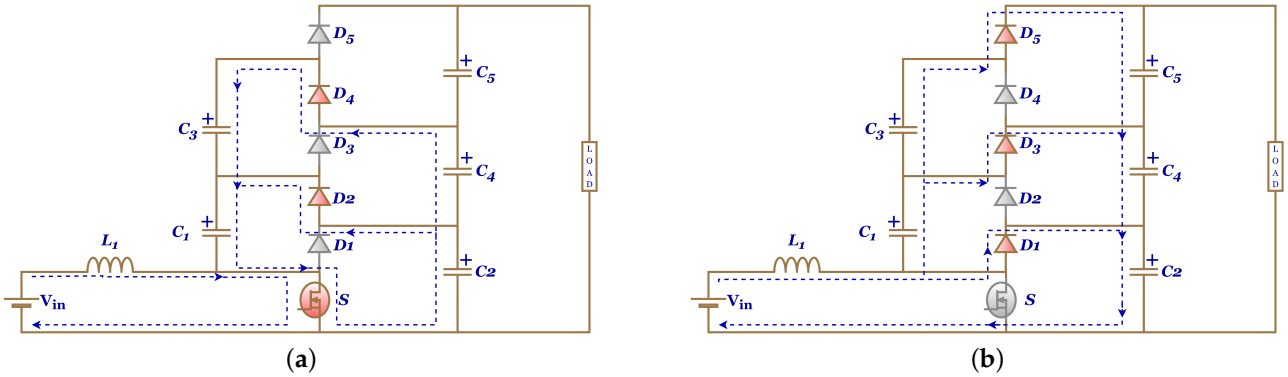

Figure 5. TBC operation: (**a**) *S* closed and (**b**) *S* open.

3.2. 1st Modified-Triple-Level Boost Converter (1st M-TBC)

One of the solutions to obtain a high voltage gain converter is presented by implementing a voltage-lift switched inductor structure that replaces the inductor in TBC to develop a new converter that contains high voltage gain, where this circuit consists of two inductors L_1 and L_2, one capacitor C_x, and two diodes D_{11} and D_{12}. The 1st M-TBC is suitable for utilization with renewable energy sources for a wide range of input voltages. The circuit of 1st M-TBC illustrated in Figure 6, which is separated into two states [16].

1. When the switch S is closed, the inductors L_1 and L_2 are connected in parallel through diodes D_{11} and D_{12} when operating in forward bias for charging. If the voltage across C_2 is smaller than C_1, C_1 will be charged from C_2 through D_2, which operates in forward bias. At the same time, the voltage across C_1 + C_3 equals the voltage across C_2+C_4, C_2 and C_4 act as a voltage source to charge C_1 and C_3 through the diode D_4, as indicated in Figure 6a.
2. When the switch S is open, the inductors L_1 and L_2 are connected in series through capacitor C_x. The diode D_1 operates in forward bias allowing the energy stored in the inductors to start the charges capacitor C_2. Furthermore, D_3 operates in forward bias, the input voltage, the inductors, and capacitors C_x and C_1 supply the capacitors C_2 and C_4. When the voltage on C_2 + C_4 is equal to the total voltage on the input voltage, the inductors voltage, and the capacitor voltage C_1 through D_5 operates in forward bias, the input voltage, inductor, and capacitors C_x, C_1, and C_3 charge capacitors C_2, C_4 and C_5 as demonstrated in Figure 6b.

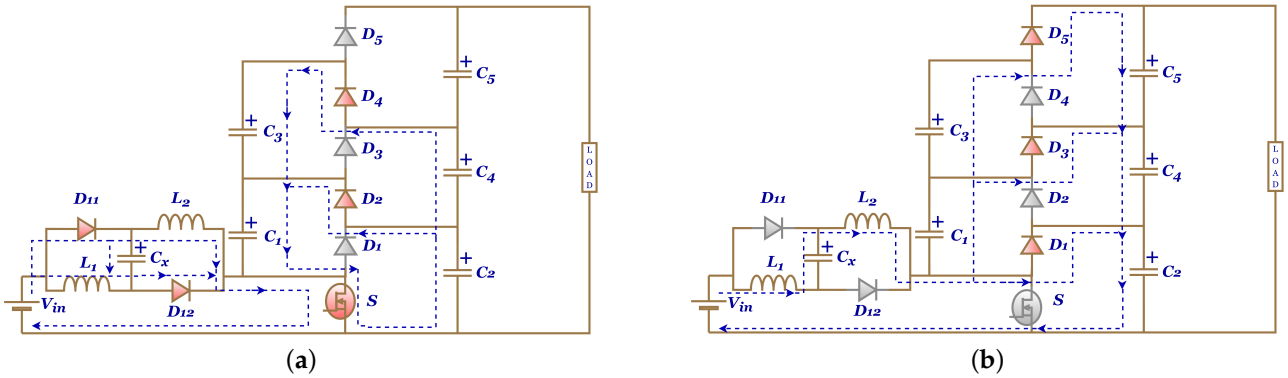

Figure 6. 1st M-TBC operation: (**a**) *S* closed and (**b**) *S* open.

The selection values of the inductors and capacitors depend on equations that are illustrated in Table 1 for calculating 1st M-TBC parameters. It is assumed that capacitors C_1, C_2, C_3, C_4, and C_5 are equal. In addition, the inductors L_1 and L_2 assumed are equal.

3.3. Double-Boost Converter (DuBC)

To improve the efficiency of conventional boost converter voltage gain and solve the problems of output voltage ripple and robustness, this paper proposes a double-boost converter (DuBC). Figure 7 illustrates the converter consisting of two power switches S_1 and S_2, two inductors L_1 and L_2, three diodes D_1, D_2, and D_3, and an output filter capacitor C_o. The two switches in the converter operate together without phase shift during the close and open states; furthermore, this converter operates in two states [45].

1. When switches S_1 and S_2 are closed, the inductors L_1 and L_2 charge from the voltage source. The input voltage,V_{in} ,charges the inductor L_1 through the switch S_1 to form the first loop and charges the inductor L_2 through diode D_1 and the switch S_2 to form the second loop. In addition, the capacitor C_o delivers power to the load, as shown in Figure 7a.
2. Figure 7b illustrates the second state of converter operation when switches S_1 and S_2 are open. The input power source V_{in} and inductors L_1 and L_2 are connected in series through diodes D_2 and D_3 that operate in forward bias to provide energy to the load and charge capacitor C_o.

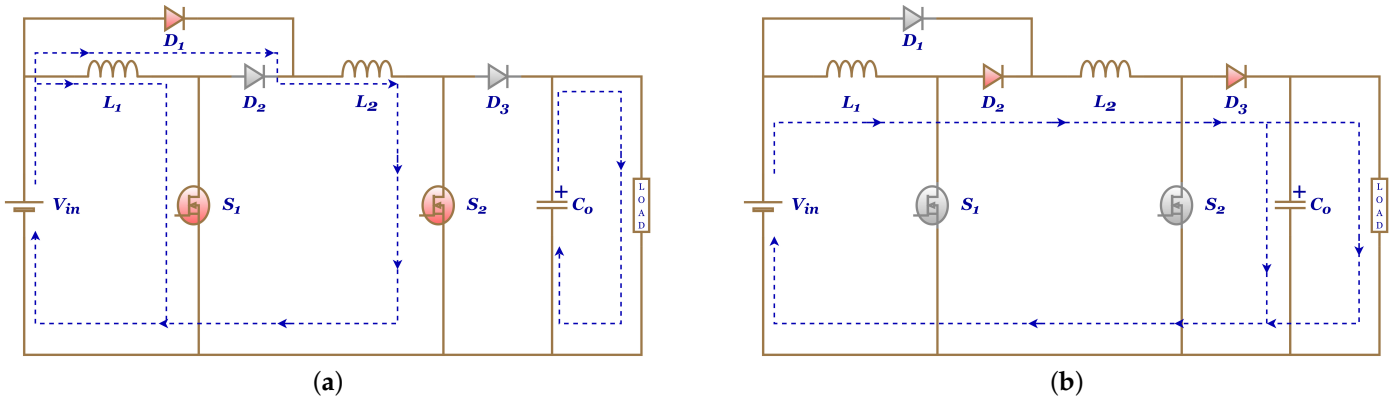

Figure 7. DuBC operation: (**a**) *S* closed and (**b**) *S* open.

The inductors and capacitor selection values depend on equations that illustrates in Table 1 for calculating DuBC parameters. It is assumed that the inductor values, L_1 and L_2, are equal.

3.4. Three-Level Boost Converter (TLBC)

To compensate for the drawbacks of the conventional boost converter. The three-level boost converter (TLBC) was developed and widely used for the hybrid hydrogen-fuel-cell railway system because the converter demonstrates low switching loss and can work with higher switching frequency. TLBC comprises two switches S_1 and S_2 and two diodes D_1 and D_2. Nevertheless, the TLBC utilizes a single input inductor L and adopts two output capacitors C_1 and C_2 to generate three-level voltage. The switches operate with a 180° phase shift to minimize current ripple [17]. The circuit of TLBC illustrated in Figure 8, which is separated into two states.

1. When S_1 and S_2 are closed. The current flow through the inductor L, which begins the charge with D_1 and D_2 operating in reverse bias. In addition, the output capacitors C_1 and C_2 discharge the current as much as the output current, as shown in Figure 8a.
2. As indicated in Figure 8b, the operation of switches that appeared S_1 is set closed and S_2 is changed to open status. The current flow from the inductor L, which began the discharge to the load and charge C_2 with D_2 operates as forward bias, while C_1 still discharge to the load. The output voltage is twice as large as the input voltage because the duty is over 0.5.

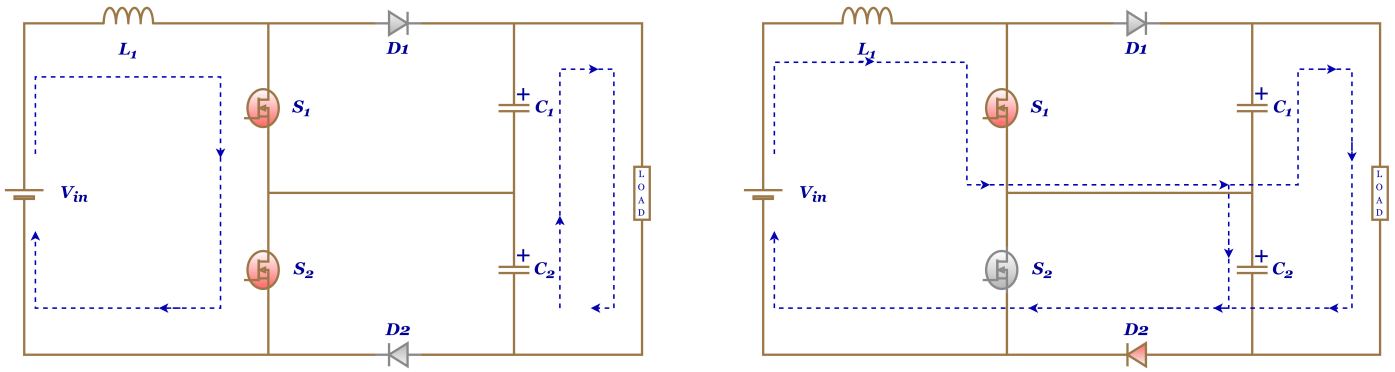

Figure 8. TLBC operation: (**a**) S_1 and S_2 closed, and (**b**) S_1 closed.

The selection values of the inductors and capacitors depend on equations that are illustrated in Table 1 for calculating TLBC parameters. The capacitors C_1 and C_2 assumed are equal.

3.5. First Modified Three-Level Boost Converter (1st M-TLBC)

With the aim to widen the step-up voltage gain of the TLBC, the diode rectification quasi-Z (DRqZ) source circuit represents another modified energy storage circuit configuration that has been suggested in combination with TLBC to achieve a high gain converter [18]. It acts as a key that can decrease the voltage stress of all semiconductors to half of the output voltage. It also has a common ground for the input and output by using the flying-capacitor three-level structure and balancing the voltage of the flying capacitor without extra circuit. Furthermore, the duty cycle operation of power switches ranged (from 0.5 to 0.75), which produces a vaster scope of voltage gain. The switches operate with a 180° phase shift to minimize current ripple. Figure 9 illustrates the circuit diagram of the 1st M-TLBC that is separated into three states of operation regain.

1. Figure 9a illustrates the 1st M-TLBC circuit when S_1 is open and S_2 is closed. This state is divided into three loops where energy flows in the circuit. To begin with, L_2 discharge to start charge C_2 through D_1 operates as forward bias. The loop 2, L_1 in series with V_{in} for supplying to charge C_1 when D_2 is forward bias. The S_2, D_1, and D_2 are ON states that appear C_{FLY} in charge operation while L_1, L_2, and V_{in} in discharge mode represent loop 3.
2. When S_1 is closed and S_2 is open, also in this state three paths of energy, the first two paths same as in the previous state. The difference in loop 3 is depicted as C_{FLY} in series with L_1, L_2, and V_{in} at discharge mode for supplying the load and charge C_o when D_3 operates in forward bias, as shown in Figure 9b.
3. The last state of operating in this converter is when S_1 and S_2 are closed, which includes two loops of energy flow. The first loop, C_1 in series with V_{in} to charge L_1 with D_1 operates in reverse bias. Similarly, C_2 transfers energy to L_2 through S_1 and S_2 in loop 2. Moreover, C_o in discharge mode to supply the load, as shown in Figure 9c.

The selection values of the inductors and capacitors depend on equations that are illustrated in Table 1 for calculating 1st M-TLBC parameters. The capacitors C_1 and C_2 assumed are equal, also inductors L_1 and L_2 are equal.

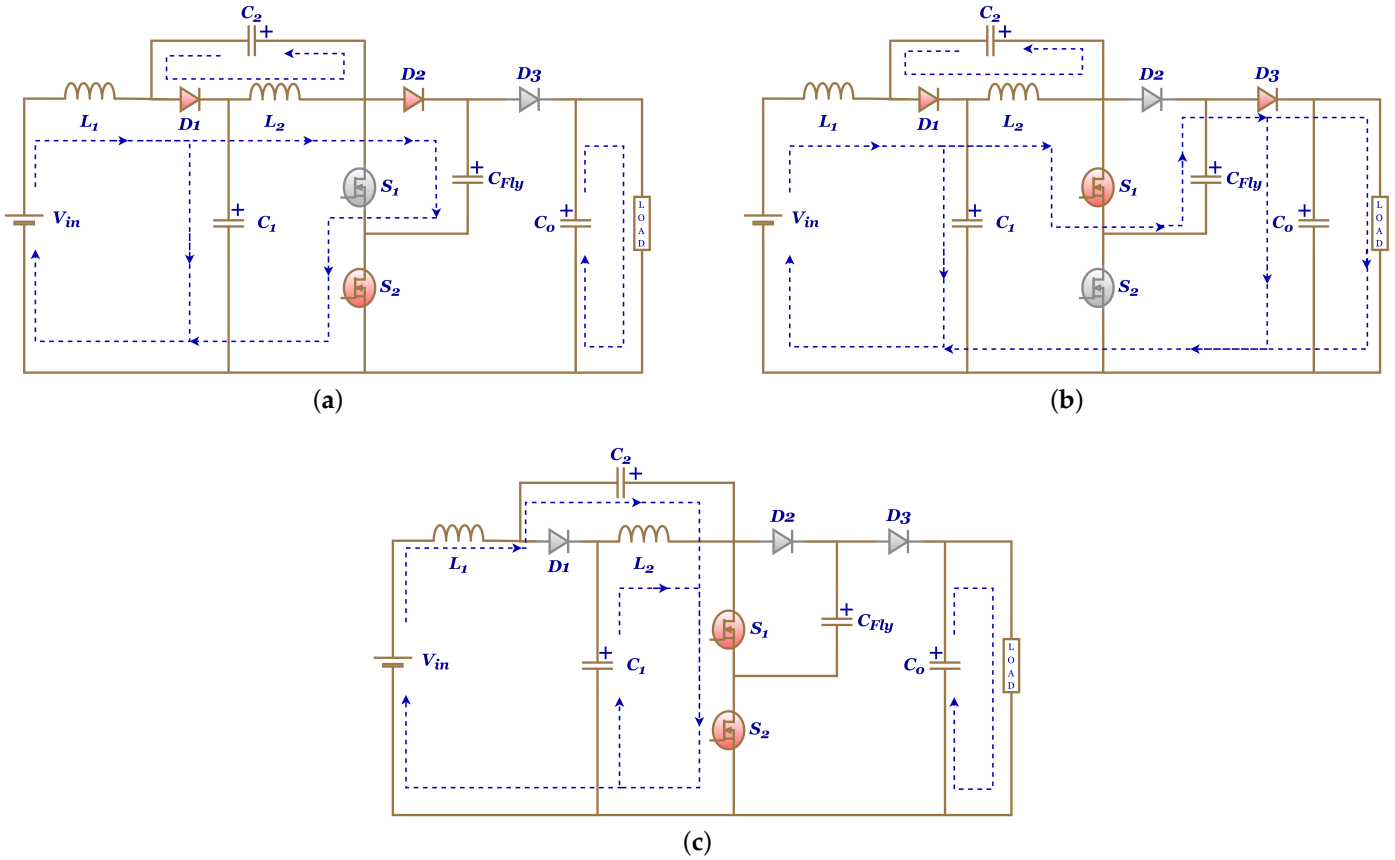

Figure 9. 1st M-TLBC operation: (**a**) S_2 closed, (**b**) S_1 closed, and (**c**) S_1 and S_2 closed.

3.6. Second Modified Three-Level Boost Converter (2nd M-TLBC)

The main disadvantage of the previous converter is that the duty cycle range is limited between 0.5 and 0.75, causing the converter to be sensitive when changes are applied to the duty cycle values. The proposed new converter is based on restructuring the 1st M-TLBC converter to achieve a voltage-balancing controller [19]. It has a high voltage conversion ratio and lower voltage stress on its power switches and diodes. The switches operate with a 180° phase shift to minimize current ripple. Figure 10 depicts a circuit diagram of the 2nd M-TLBC that is separated into four conditions of operation regain.

1. Two current loops appear when S_1 is open, and S_2 is closed, as depicted in Figure 10a. Loop 1: L_1 connected in series with V_{in} to charge C_2, when D_1 is in forward bias. L_2 and C_3 supply current to charge C_1 and C_2. Furthermore, D_3 operates as a forward bias to supply the C_o and the load representing loop 2.
2. Figure 10b illustrates the second operation state when S_1 is closed, and S_2 is open. The V_{in}, L_1, and C_2 in series for supplying current to charge C_3 through D_2 operates in forward bias. loop 2 represents C_1 charge from L_2 and C_2 through D_2 operates in forward bias. In addition, D_3 operates as a forward bias to supply the C_o and the load.
3. The third state of switches is where S_1 and S_2 are closed. The source V_{in} supplies current to charge L_1 is depicted as loop 1. The power diodes are in reverse bias, so L_2 and C_3 supply the C_3. The C_o in discharge mode to supply the load, as shown in Figure 10c.
4. Final state where S_1 and S_2 are open states and all power diodes are in forward bias, the V_{in} in series with L_1 discharge to supply C_3, while L_2 charge from C_1 . In addition, D_3 operates as a forward bias to supply the C_o and the load. Which describes two loops illustrated in Figure 10d.

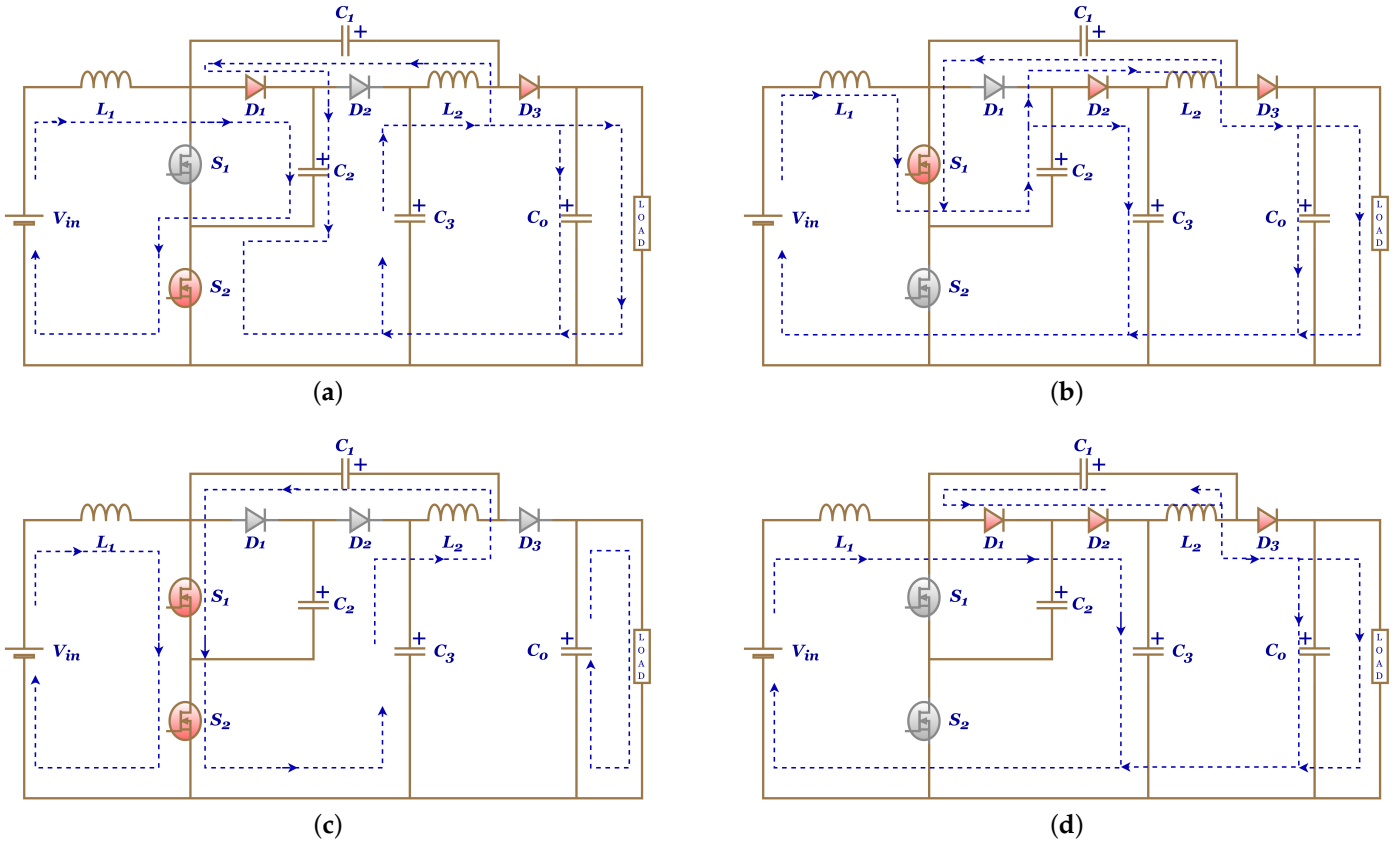

Figure 10. 2nd M-TLBC operation: (**a**) S_2 closed, (**b**) S_1 closed, (**c**) S_1 and S_2 closed, and (**d**) S_1 and S_2 open.

The selection values of the inductors and capacitors depend on equations that are illustrated in Table 1 for calculating 2nd M-TLBC parameters. The capacitors C_1, C_2 and C_3 assumed are equal, moreover, inductors L_1 and L_2 are equal.

3.7. Interleave Boost Converter (IBC)

The interleaved structure is one of the practical solutions to boost the power level, which can reduce the current ripple, decrease the passive component size, enhance the transient response, and realize the thermal distribution [46]. The simplicity is a significant feature of interleave topology because the interleaved boost converter cells share the input current, so the current ripples are small, which maintains the life of FC stacks [47]. Interleaved boost converter consists of "n" single boost converters connected in parallel. In the simulation, there is no boundary for the number of interleaved power branches' legs. Through practical implementation, as the phase number increases, the system complexity increases, and maintenance becomes problematic. The input/ EMI filter and output capacitor sizes are reduced proportionally with the ripple reduction. The disadvantage of the interleaving approach is the rise in gate driving logic complexity, but perhaps more significantly, the size and cost of the gate drive [48]. The phase-shifted applied for the operation of the switches on the gates defined as

$$\theta = \frac{360^\circ}{n} \tag{2}$$

where n is the number of phases chosen for the interleave boost converter [20,21,47].

3.7.1. Two Phase Interleave (2-IBC)

Figure 11 illustrates the operation of 2-IBC, which is separated into two states and contains two modes. The phase shifts between each switch are 180° because n equals two depending on Equation (2) [20,21,47].

1. Mode 1: When S_1 is closed and S_2 is open. The current through L_1 began to rise, and L_2 began to discharge to load with D_2 operating as forward bias, as shown in Figure 11a.
2. Mode 2: When S_1 and S_2 are open. The current discharges through the output circuit from L_1 and L_2 to load with D_1 and D_2 operating as forward bias, as shown in Figure 11b.

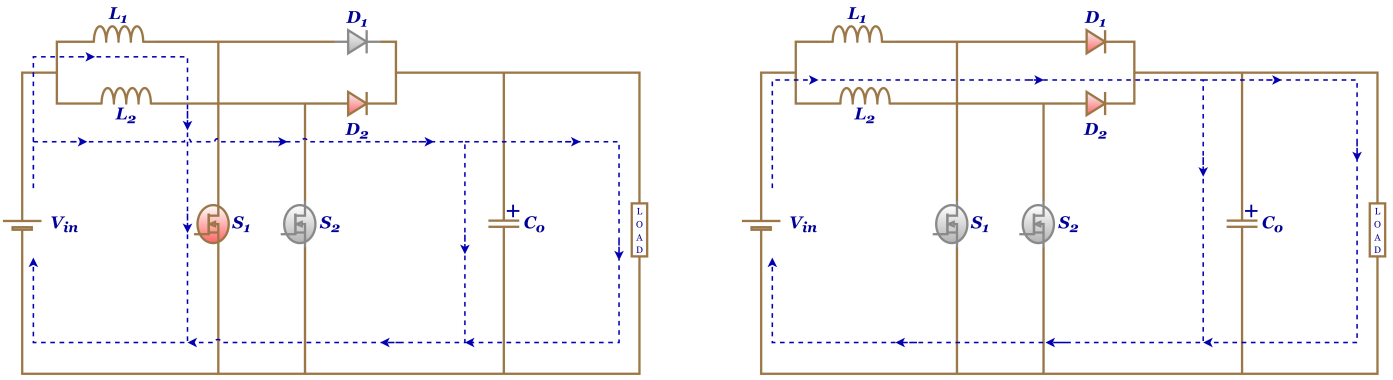

Figure 11. 2-IBC operation: (**a**) S_1 closed, and (**b**) all switches open.

Due to the symmetry of the circuit, the state II of the analysis is similar to the previous. Modes 3 and 4 are similar to modes 1 and 2.

The selection values of the inductors and capacitors depend on equations that are illustrated in Table 1 for calculating 2-IBC parameters. The inductors L_1 and L_2 assumed are equal.

3.7.2. Four Phase Interleave (4-IBC)

In maintaining the life of FC, researchers should focus on reducing the current ripple because of a significant issue. A way to overcome this problem is using polyphase operation with suitable phase shifts in the control circuit of main switches. Figure 12 illustrates the operation of 4-IBC, which is separated into four states and contains two modes. The phase shifts between each switch are 90° because n equals four depending on Equation (2) [20,21,47].

1. Mode 1: when S_1 is closed. S_2, S_3, and S_4 are open. The current through L_1 began to rise, and L_2, L_3, and L_4 began to discharge to load with D_2, D_3, and D_4 operating as forward bias, as shown in Figure 12a.
2. Mode 2: When S_1, S_2, S_3, and S_4 are open. The current discharges through the output circuit from L_1, L_2, L_3, and L_4 to load with D_1, D_2, D_3, and D_4 operating as forward bias, as shown in Figure 12b.

Due to the symmetry of the circuit, the states II, III, IV of the analysis are similar to the previous. Modes 3 and 4 are similar to modes 1 and 2. Modes 5 and 6 are similar to modes 1 and 2. Furthermore, modes 7 and 8 are similar to modes 1 and 2 [22].

The selection values of the inductors and capacitors depend on equations that are illustrated in Table 1 for calculating 4-IBC parameters. The inductors L_1, L_2, L_3, and L_4 assumed are equal.

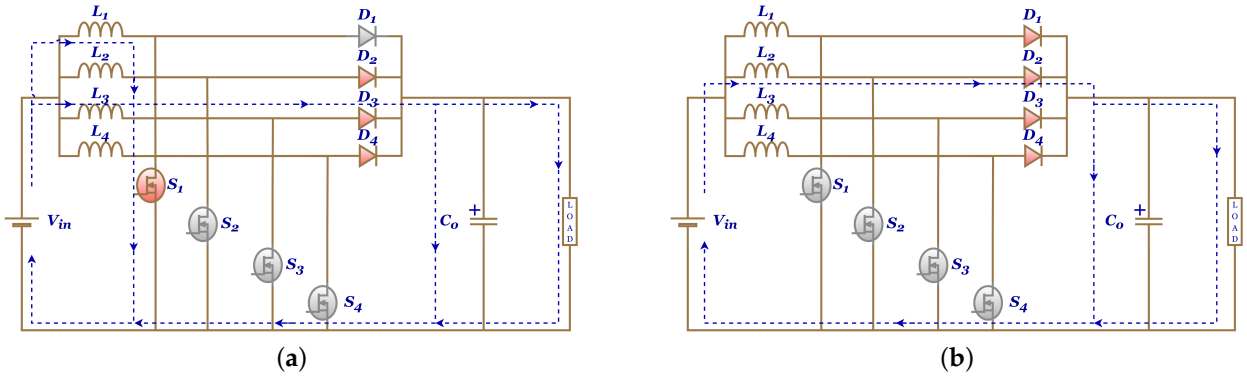

Figure 12. 4-IBC operation: (**a**) S_1 closed, and (**b**) all switches open.

3.8. First Modified-Interleave Boost Converter (1st M-IBC)

The main disadvantage of IBC topology is relatively low voltage gain. To improve voltage gain of IBC structures, they can be mixed with a voltage-doubler.The 1st M-IBC circuit proposed is similar to the conventional IBC but includes an extra capacitor C_x [23]. For operating IBC with voltage-doubler, the duty cycle value ($0.5 \leq D \leq 1$), with this topology illustrated in Figure 13, which is separated into three states.

1. During the period when switch S_1 is *OFF*, the D_1 is operates in forward bias that apply C_x to charge from L_1 as demonstrated in Figure 13a. The C_o start discharging to supply the load.
2. While the period when switch S_2 is *OFF*, the V_{in}, L_2, and C_x are connected in series to supply current to C_o, and the load through D_2 when operates as a forward bias, as indicated in Figure 13b.
3. Figure 13c illustrates that in the state of switches, when operating during the *ON* state, the L_1 and L_2 connected with V_{in} to start charging [23].

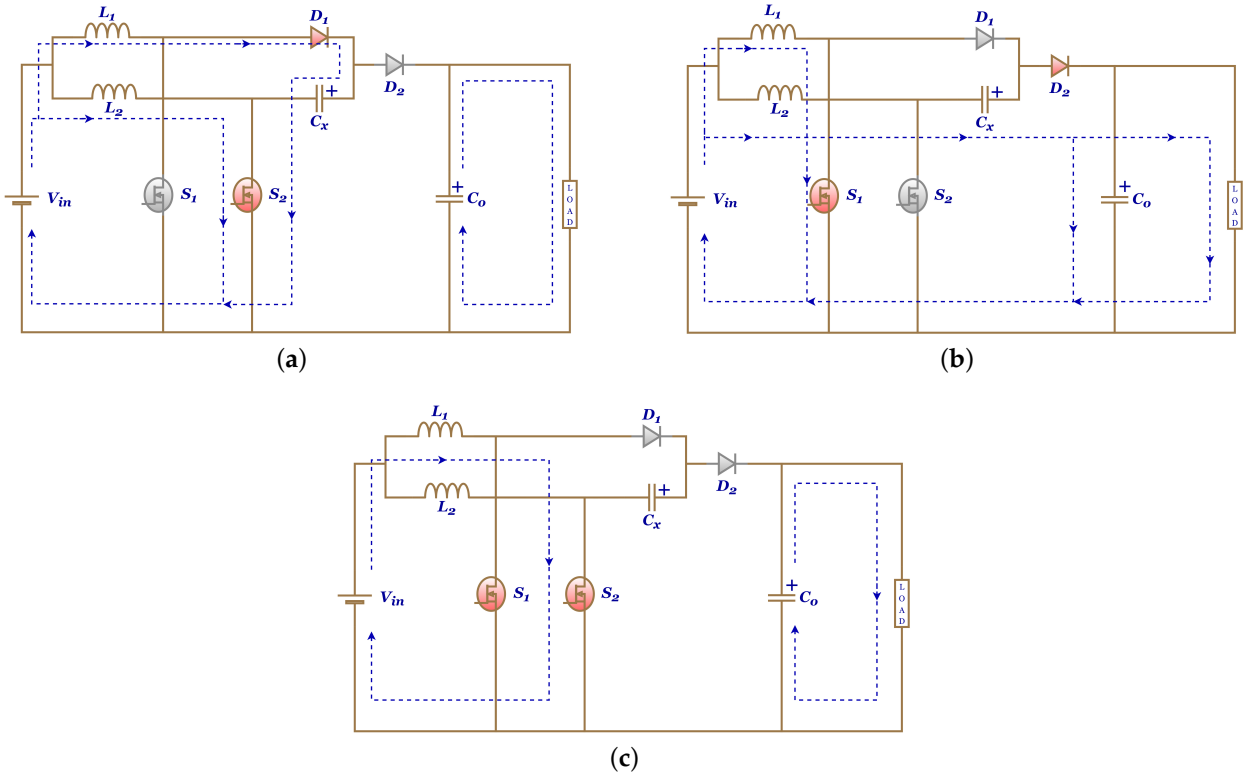

Figure 13. 1st M-IBC operation: (**a**) S_2 closed, (**b**) S_1 closed, and (**c**) S_1 and S_2 closed.

The selection values of the inductors and capacitors depend on equations that are illustrated in Table 1 for calculating 1st M-IBC parameters.

3.9. Second Modified-Interleave Boost Converter (2nd M-IBC)

Based on previous modifications of IBC, this study proposed the implementation of another voltage-doubler circuit, the voltage conversion ratio is enlarged, and the substantial duty ratio can be avoided in the high step-up applications. Moreover, the voltage stress of all the power devices is significantly lower than the output voltage. As a result, lower-voltage-rated power devices can be employed, and higher efficiency can be expected. This converter is utilized based on the IBC structure containing two power switches S_1 and S_2, which operate with 180° phase-shift separated into three operation states [24].

1. As shown in Figure 14a, switches S_1 and S_2 are closed, and the inductors L_1 and L_2 start charging. Meanwhile, all power diodes in this circuit operate in reverse bias. The C_o start discharging to supply the load.
2. When S_1 is closed, L_2 is discharged for charging C_1 through D_1 operates in forward bias, whereas L_1 is still charging, as shown in Figure 14b. Moreover, the L_2 and C_2 are in series to supply the load and charge C_o when D_3 operates in forward bias.
3. When S_2 is closed, L_1 and C_1 are discharged for charging C_2 through D_2 operates in forward bias and supply the load and charge C_o through D_3 operates in forward bias, whereas L_2 is still charging, as shown in Figure 14c.

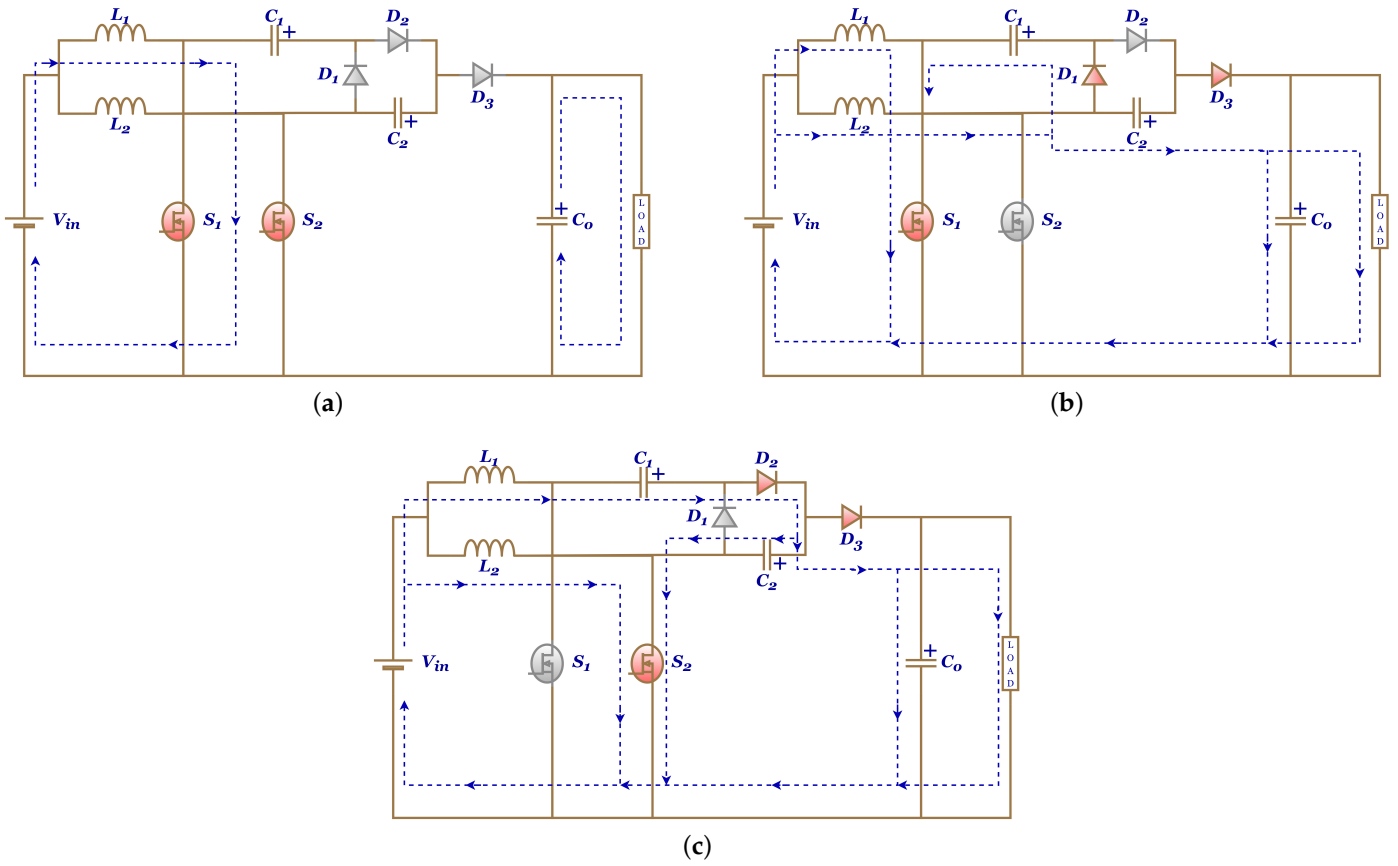

Figure 14. 2nd M-IBC operation: (**a**) S_1 and S_2, (**b**) S_1 closed, and (**c**) S_2 closed.

The selection values of the inductors and capacitors depend on equations that are illustrated in Table 1 for calculating 2nd M-IBC parameters. The capacitors C_1 and C_2 assumed are equal. Furthermore, L_1 and L_2 assumed are equal.

3.10. Third Modified-Interleave Boost Converter (3rd M-IBC)

An interleaved high-gain topology with a simple configuration, effortless control, and diminished switch stress is proposed in this study. Figure 15 illustrates this converter circuit that consists of two inductors L_1 and L_2, three capacitors C_1, C_2, and C_o, two switches S_1 and S_2, and three diodes D_1, D_2, and D_3. The switches function synchronously, facilitating the control of the converter, which is split into two states of operation regain [25].

1. When switches S_1 and S_2 are closed, the inductor L_1 starts to charge from the source V_{in}, whereas L_2 starts charging by V_{in} and C_1. Furthermore, the capacitor C_2 charge from V_{in} and C_1 when diode D_2 operates in forward bias. The load energy is supplied by C_o, as shown in Figure 15a.
2. Figure 15b displays the open state of the switches. The inductor L_1 with V_{in} charge capacitor C_1 via D_1 operates in forward bias. Moreover, inductor L_2, V_{in}, and C_2 flow energy to the load, and capacitor C_o via D_3 operates in forward bias.

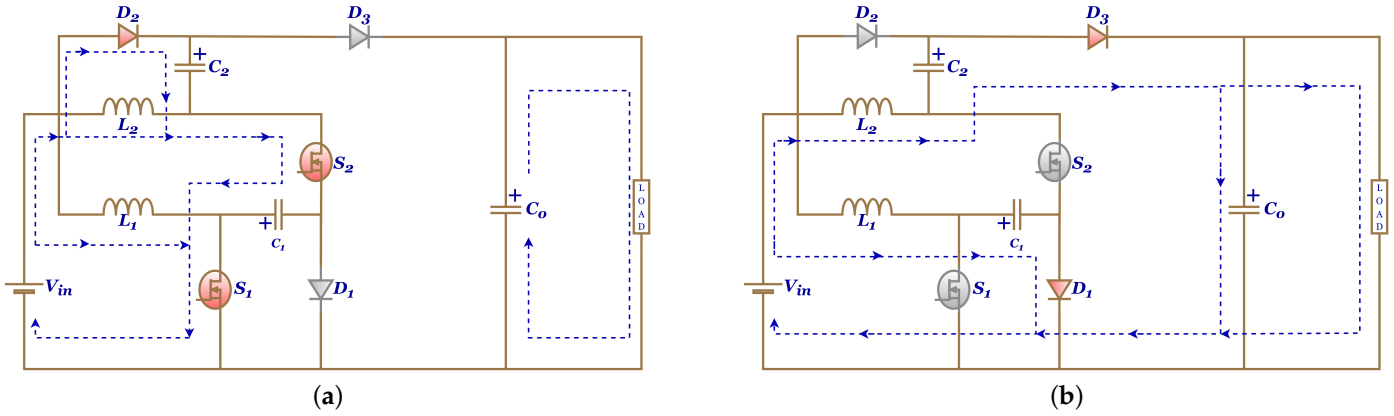

Figure 15. 3rd M-IBC operation: (**a**) S_1 and S_2 closed, and (**b**) S_1 and S_2 closed.

The selection values of the inductors and capacitors depend on equations that are illustrated in Table 1 for calculating 3rd M-IBC parameters.

3.11. Positive Output Super-Lift (PSOL)

One of the advantages of applying the voltage-lift technique is being able to achieve a high-voltage gain converter. This study proposed a new converter with a high voltage gain, reduced voltage stress, and increased reliability called Positive Output Super lift (PSOL) [26]. The PSOL consists of one inductor, two capacitors, two power diodes, and one power switch. Figure 16 depicts the circuit diagram of the PSOL that is split into two states of operation regain.

1. When S operates during the *ON* state, the current flow charging L_1 and C_1 through the D_1 operate forward biased, while C_o supply current to the load at this state as shown in Figure 16a.
2. Figure 16b, at the second condition of S, L_1 and C_1 discharge to provide current to C_o and the load when D_2 operates at forward bias.

The selection values of the inductors and capacitors depend on equations that are illustrated in Table 1 for calculating PSOL parameters.

3.12. First Modified-Positive Output Super-Lift (1st M-PSOL)

The proposed modification of PSOL is explained in Figure 17. The 1st M-PSOL scheme is built by replacing the inductor L with the switched-inductor structure that consists of two inductors L_1 and L_2, and three diodes D_1, D_2, and D_3 . The inductors L_1 and L_2 can be separated or magnetically coupled to shape for more efficient use [27]. The 1st M-PSOL split into two states of operation regain.

1. When S is closed, the L_1, L_2, and C_1 are connected in parallel through D_1, D_3, and D_4 when operating forward bias for start charge from the supply; furthermore, C_o discharge to deliver the current to load, as shown in Figure 17a.
2. When S is open, Figure 17b illustrates the state of L_1, L_2 ,and C_1 when starting discharge for charge C_o and supplying the load through D_2 and D_5 when operating forward bias.

The 1st M-PSOL selection values of the inductors and capacitors depend on equations that are illustrated in Table 1, where L_1 and L_2 are assumed equal.

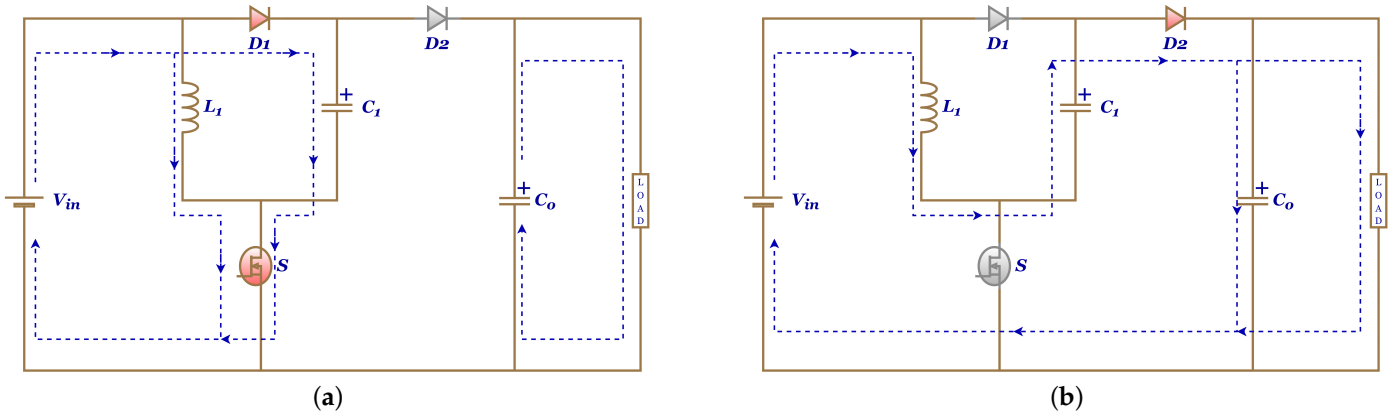

Figure 16. PSOL operation: (**a**) *S* closed, and (**b**) *S* open.

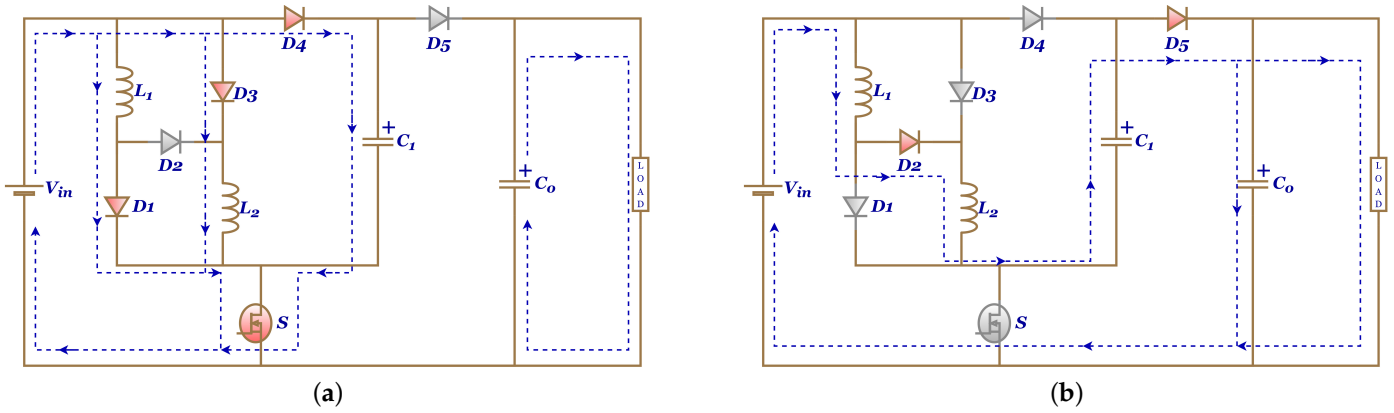

Figure 17. 1st M-PSOL operation: (**a**) *S* closed, and (**b**) *S* open.

3.13. Second Modified-Positive Output Super-Lift (2nd M-PSOL)

For the aim to increase voltage gain, this study proposed a change structure in the previous converter by replacing D_2 with a new capacitor C_x as shown in Figure 18 [28]. The 2nd M-PSOL split into two states of operation regain.

1. Figure 18a illustrates the *ON* state of switch S; when D_1, D_2, and D_3 operate forward biased, the storage elements L_1, and L_2 are connected in parallel with the source to start charge. Moreover, in this stage C_x, and C_1 start charging. The C_o discharge to supply the load.
2. When S is *OFF* condition, L_1, L_2, C_x, and C_1 discharge to supply C_o and load when connected in series through D_4 operate at forward bias, as shown in Figure 18b.

The 2nd M-PSOL inductors and capacitors selection values depend on equations that illustrates in Table 1, where assumed L_1, andL_2 are equal, also C_x, andC_1 are equal.

3.14. Third Modified-Positive Output Super-Lift (3rd M-PSOL)

This study proposed the combination of cascaded boost and Luo converters to accomplish higher values of voltage gain, which is the primary reason for the suitability of the designed converter utilization in renewable energy applications [29]. The circuit schematic of the 3rd M-PSOL topology is demonstrated in Figure 19. The first stage of the designed converter operates as a cascaded boost. Thus, a PSOL converter in the second stage operates, increasing the voltage gain. A higher voltage gain ratio became achievable with a lower duty cycle value. The 3rd M-PSOL split into two states of operation regain.

1. In the first operation mode, the switch S is *ON*. Meanwhile, the D_1 and D_3 diodes are in the forward bias. The inductors L_1 and L_2 and capacitor C_2 start charging at this state. Meanwhile, capacitors C_1 and C_o discharge, as shown in Figure 19a.
2. On the other hand, Figure 19b illustrates the second operation mode when switch S is *OFF*. The inductors L_1 and L_2 and capacitor C_2 start discharge to provide current to C_1 and C_o through D_2, and D_4 operates at forward bias.

The selection values of the inductors and capacitors depend on equations that are illustrated in Table 1 for calculating 3rd M-PSOL parameters.

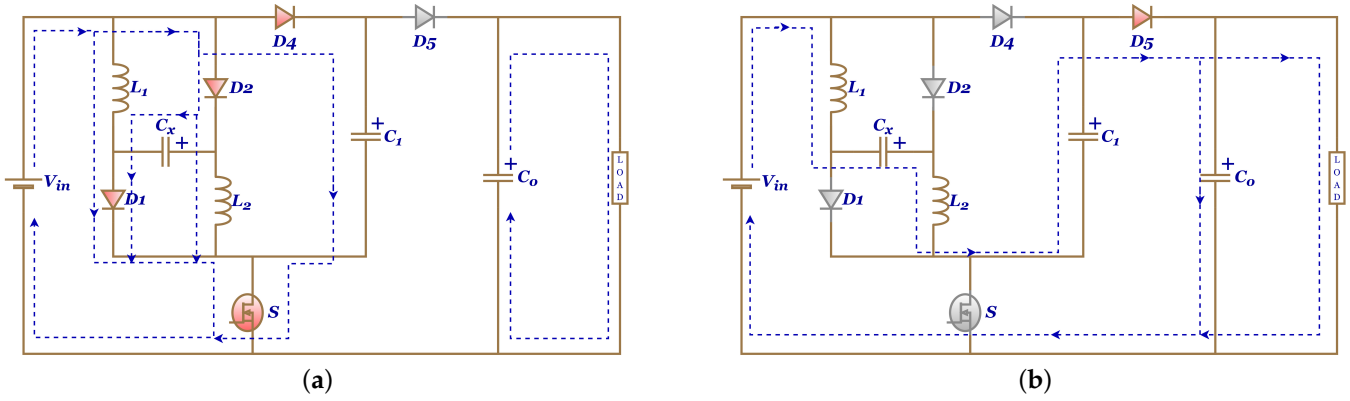

Figure 18. 2nd M-PSOL operation: (**a**) *S* closed, and (**b**) *S* open.

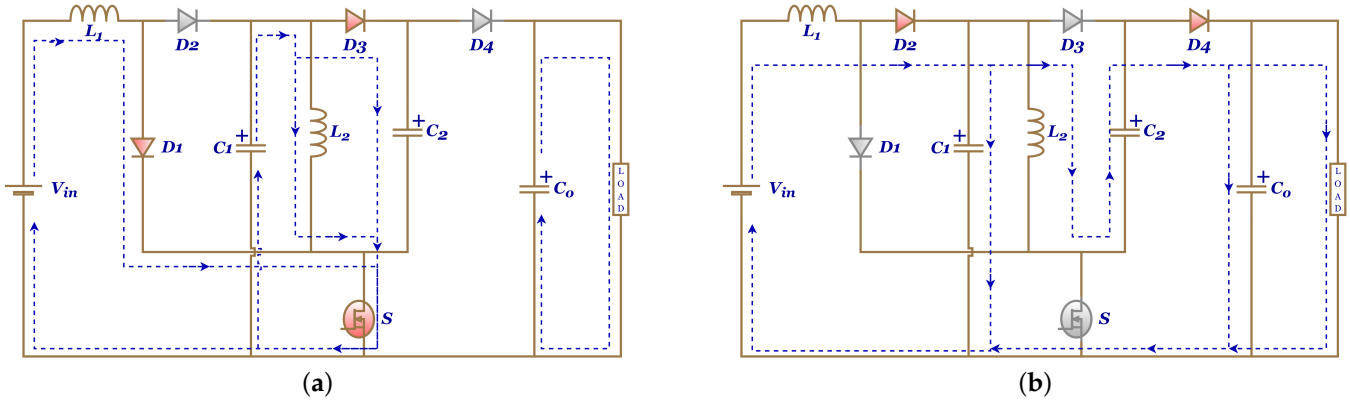

Figure 19. 3rd M-PSOL operation: (**a**) *S* closed, and (**b**) *S* open.

3.15. Fourth Modified-Positive Output Super-Lift (4th M-PSOL)

Another integration of the PSOL converter with the Cuk converter is proposed in this study to reach high voltage gain [30]. The circuit schematic of the 4th M-PSOL topology is demonstrated in Figure 20, where the two switches S_1 and S_2 operate simultaneously without any phase shift between these switches. The first stage of the conceived converter operates as a Cuk converter. Hence, a PSOL converter in the second stage operates, raising the voltage gain. The 4th M-PSOL split into two states of operation regain.

1. Figure 20a illustrates the first state of operation of the 4th M-PSOL, where S_1, S_2, and D_1 operate during the *ON* state condition. Due to this condition, C_1 and C_2 have become parallel. Consequently, their voltage has become equal to each other. The parallel connection of the C_1 and C_2 causes a current to fly from the C_1 to the positive terminal of the C_2 to charge this capacitor. The inductors L_1 and L_2 start charging in this state. The C_1 and C_o capacitors have become discharged by the second inductor and supply load, respectively.
2. When switches S_1 and S_2 are *OFF*. The C_1 and the C_o capacitors become charged by the flowing current of the L_1 and L_2 inductors, respectively. Furthermore, the capacitor C_2 discharge to supply the load and C_o through D_3 operates in forward bias, as shown in Figure 20b.

The selection values of the inductors and capacitors depend on equations that are illustrated in Table 1 for calculating 4th M-PSOL parameters.

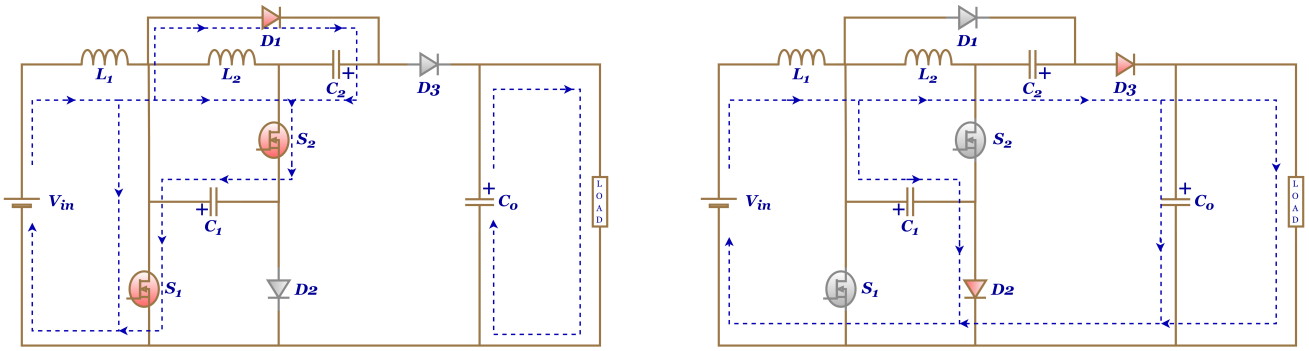

Figure 20. 4th M-PSOL operation: (**a**) S_1 and S_2 closed, and (**b**) S_1 and S_2 open.

3.16. Single-Ended Primary Inductor Converter (SEPIC)

The single-ended primary inductor converter is shown in Figure 21 and is generally referred to as a SEPIC converter. It can also step up and step down the output voltage levels. It has a non-inverting output, making it more appealing than buck-boost converters, and it is preferred for high-power applications. This setup benefits vital features such as the continuous output current, minimizing the switching stress, and output ripple, so the SEPIC converter is utilized for renewable energy applications [9]. As mentioned, SEPIC operates as the buck-boost converter; If D is less than 0.5, the converter reduces the supplied voltage and functions as a buck converter; if D is more significant than 0.5, the converter rises the given voltage and functions as a boost converter. The SEPIC split into two states of operation regain [31,32].

1. As presented in Figure 21a, switch S is closed, and the inductor L_1 gets charged by the voltage source V_{in}. In addition, the inductor L_2 takes energy from the capacitor C_1. The output capacitor C_o discharges to supply the load.
2. When switch S is open, the inductors L_1 and L_2 discharging to charge C_1, C_o, and supply the load when diode D operates in forward bias, as shown in Figure 21b.

The selection values of the inductors and capacitors depend on equations that are illustrated in Table 1 for calculating SEPIC parameters, where L_1 and L_2 assumed are equal.

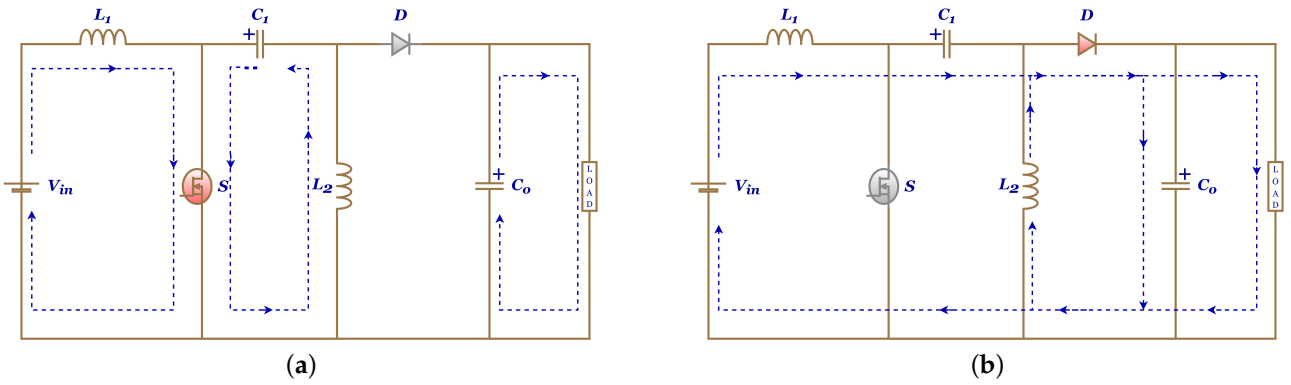

Figure 21. SEPIC operation: (**a**) *S* closed, and (**b**) *S* open.

3.17. First Modified-Single Ended Primary Inductor Converter (1st SEPIC)

This study suggested a modified SEPIC converter by adding only two components with the diode D_x and the capacitor C_x, as presented in Figure 22. This topology presents low switch voltage and high efficiency for high output voltage applications by increasing voltage gain [33]. The 1st SEPIC split into two states of operation regain.

1. When switch *S* is closed, the input voltage is applied to charge the inductor L_1, and the inductor L_2 and capacitor C_1 start charging form the C_x. While C_o discharge to supply the load, as shown in Figure 22a.
2. Figure 22b illustrates the open state of switch *S*; the L_1 and C_1 discharge to load through diode D_1 when operating in forward bias. Furthermore, the capacitor C_x start charge through the diode D_x when operating in forward bias. The inductor L_2 is discharged to load through diode D_1.

The selection values of the inductors and capacitors depend on equations that are illustrated in Table 1 for calculating 1st M-SEPIC parameters, where L_1 and L_2 assumed are equal, and C_x and C_1 assumed are equal.

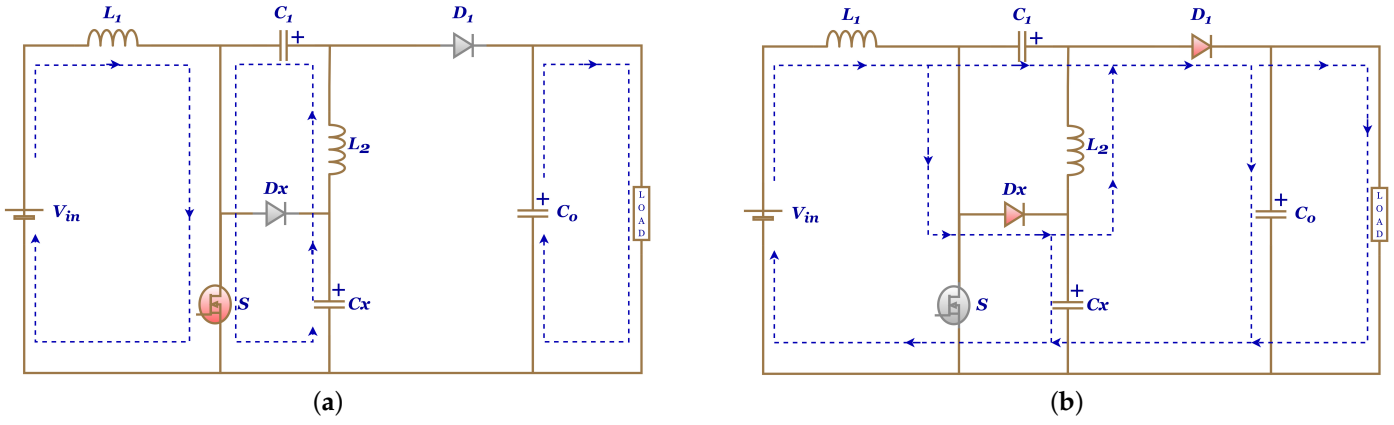

Figure 22. 1st M-SEPIC operation: (**a**) *S* closed, and (**b**) *S* open.

3.18. Second Modified-Single Ended Primary Inductor Converter (2nd M-SEPIC)

Based on a previous modification of the SEPIC converter, this study proposed utilizing a combination of 1st M-SEPIC with switched capacitor circuit for achieving a new modification of SEPIC to reach a high voltage conversion ratio. The switched capacitor structure consists of two capacitors C_3 and C_4, and two diodes D_2 and D_3 [34]. The 2nd M-SEPIC split into two states of operation regain, as shown in Figure 23.

1. As shown in Figure 23a, switch S is closed. The input voltage is applied to charge the inductor L_1, and the L_2 and C_1 start charge from the C_2. Through D_3 is forward bias C_3 start charge from C_4 and C_o supply the load .
2. When switch S is open, the L_1, and C_1 discharge to load through D_4. Furthermore, L_2 charges from source, L_1, and C_1. While, C_2, C_4, C_o start charging when D_1, D_2, and D_4 operating as forward bias, as shown in Figure 23b.

The 2nd M-SEPIC calculated value parameters are illustrated in Table 1. Where inductors L_1 and L_2 are assumed equal. Furthermore, capacitors C_1, C_2, C_3, and C_4 are assumed equal.

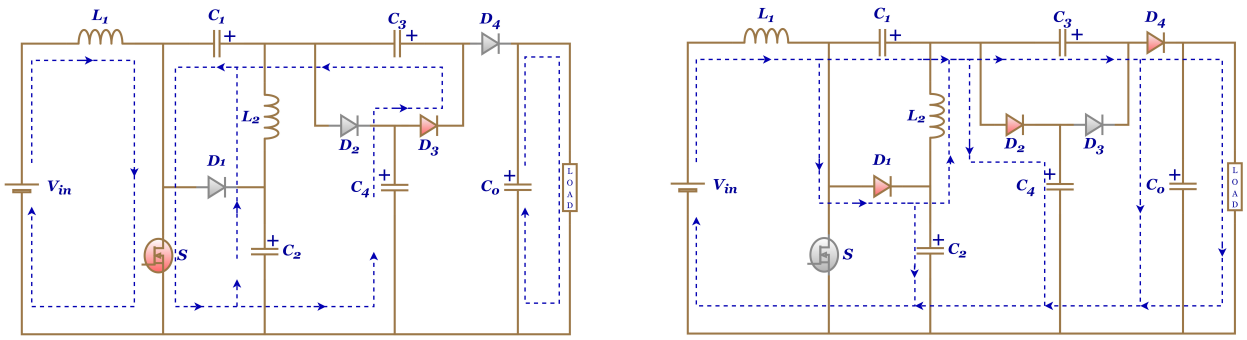

(**a**) (**b**)

Figure 23. 2nd M-SEPIC operations (**a**) S closed (**b**) S open.

3.19. Third Modified-Single Ended Primary Inductor Converter (3rd M-SEPIC)

This paper proposed a modified SEPIC converter to achieve high static gain together with maintaining low-input current ripples inherently. Moreover, the switching losses and stress are significantly reduced due to low-input current ripples. The modification is achieved based on 1st M-SEPIC with replacement L_1 by utilizing a switch-inductor circuit that consists of two inductors L_1 and L_2, and three diodes D_1, D_2, and D_3. The 3rd M-SEPIC split into two states of operation regain, as shown in Figure 24 [35].

1. When S is turned on, the inductors L_1 and L_2 are connected parallel to the source voltage through forward-biased diodes D_1 and D_3. At the same time, capacitors C_1 and L_3 are charged from C_2 via switch S at closed state. The load is driven by an output voltage across capacitor C_o, as shown in Figure 24a.
2. In this mode, switch S is turned off. The inductors L_1 and L_2 are now connected in series via forward-biased diode D_2. After that, inductors L_1, L_2, and L_3 are discharging linearly, whereas capacitors C_1, C_2, and C_o are charging via forward-biased diodes D_4 and D_5, as shown in Figure 24b.

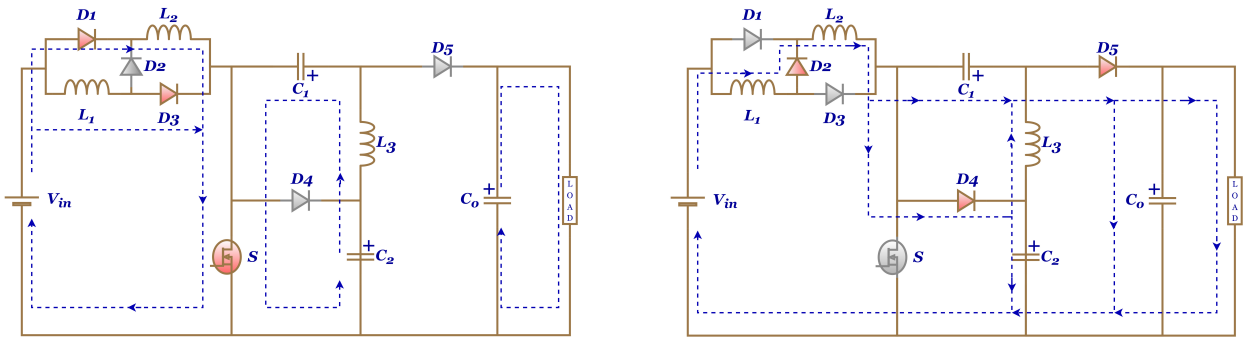

(**a**) (**b**)

Figure 24. 3rd M-SEPIC operations (**a**) S closed (**b**) S open.

The 3rd M-SEPIC calculated value parameters are illustrated in Table 1. Where inductors L_1, L_2, and L_3 are assumed equal, and capacitors C_1 and C_2 are also assumed equal.

3.20. Fourth Modified-Single Ended Primary Inductor Converter (4th M-SEPIC)

The voltage gain ratio is still limited, so this study proposed a new modification of the SEPIC converter that combines 2nd M-SEPIC and 3rd M-SEPIC converter to reach higher conversion with a low-duty cycle. Figure 25 depicts the 4th M-SEPIC circuit, which operates in two states [36].

1. When S is closed, the inductors L_1 and L_2 are connected parallel to the source voltage through forward-biased diodes D_1 and D_3. At the same time, the L_3 and C_1 charge from the C_2. Through D_6 is forward bias C_3 start charge from C_4 and C_o supply the load .
2. When switch S is open, the inductors L_1 and L_2 are now connected in series via forward-biased diode D_2. After that, capacitor C_2 start charge when D_4 operates as forward bias. The inductor L_3 in this state discharge to supply the load in same currnt path of L_1 and L_2. In contrast, capacitor C_4 start charging through D_5 from C_4. While C_3 discharge to load and charge C_o, as shown in Figure 25b.

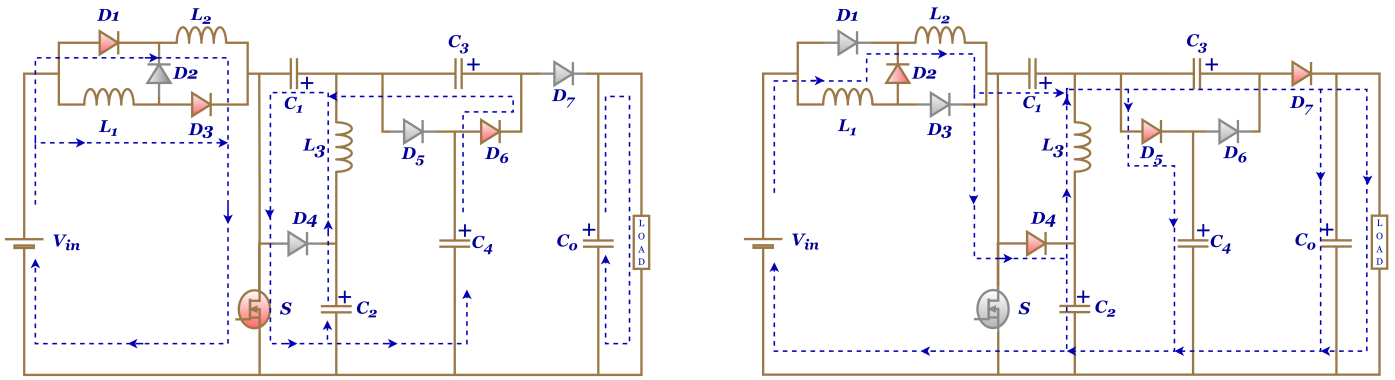

Figure 25. 4th M-SEPIC operations (**a**) S closed (**b**) S open.

The 4th M-SEPIC calculated value parameters are illustrated in Table 1. Where inductors L_1, L_2, and L_3 are assumed equal. Furthermore, capacitors C_1, C_2, C_3, and C_4 are assumed equal.

Table 1 illustrates the equations employed to design these converter parameters and the value of these parameters for each converters type, when assumed duty cycle D = 0.5, the input voltage V_{in} = 24 V, switching frequency f_s = 25 kHz, inductor ripple current ΔI_L = 10% of input current, and output voltage ripple ΔV_o = 5% of output voltage.

Table 1. Analytical equations for component parameter design.

Converter Type	Equations		Parameters	
	Inductors	**Capacitors**	**Inductors**	**Capacitors**
DBC	$L = \frac{V_{in} \cdot D}{f_s \cdot \Delta i_L}$	$C = \frac{V_o \cdot D}{f_s \cdot \Delta V_o \cdot R}$	$L_1 = 100\,\mu H$	$C_1 = C_2 = C_3 = C_4 = 4.5\,\mu F$
TBC	$L = \frac{V_{in} \cdot D}{f_s \cdot \Delta i_L}$	$C = \frac{V_o \cdot D}{f_s \cdot \Delta V_o \cdot R}$	$L_1 = 100\,\mu H$	$C_1 = C_2 = C_3 = C_4 = C_5 = 4.5\,\mu F$
1st M-TBC	$L = \frac{V_{in} \cdot D}{f_s \cdot \Delta i_L}$	$C = \frac{V_o \cdot D}{f_s \cdot \Delta V_o \cdot R}$	$L_1 = L_2 = 100\,\mu H$	$C_1 = C_2 = C_3 = C_4 = C_5 = 4.5\,\mu F$
DuBC	$L = \frac{V_{in} \cdot D}{2 \cdot f_s \cdot \Delta i_L}$	$C = \frac{V_o \cdot D}{f_s \cdot \Delta V_o \cdot R}$	$L_1 = L_2 = 50\,\mu H$	$C_o = 10\,\mu F$
TLBC	$L = \frac{V_{in} \cdot (D-0.5)}{f_s \cdot \Delta i_L}$	$C = \frac{2V_o \cdot (D-0.5)}{f_s \cdot \Delta V_o \cdot R}$	$L_1 = 10\,\mu H$	$C_1 = C_2 = 0.25\,\mu F$
1st M-TLBC	$L = \frac{V_o \cdot (2D-1) \cdot (1-D)}{2 f_s \cdot \Delta i_L}$	$C = \frac{V_o \cdot (2D-1)}{(3-4D) \cdot f_s \cdot \Delta V_c \cdot R}$; $C_{F_{L_Y}} = \frac{V_o \cdot (2D-1)}{(3-4D) \cdot f_s \cdot \Delta V_c \cdot R}$; $C_o = \frac{V_o \cdot D}{f_s \cdot \Delta V_o \cdot R}$	$L_1 = L_2 = 5\,\mu H$	$C_1 = C_2 = 0.25\,\mu F$; $C_{F_{L_Y}} = 8\,\mu F$; $C_o = 10\,\mu F$
2nd M-TLBC	$L = \frac{V_o \cdot (2D-1) \cdot (1-D)}{2 f_s \cdot \Delta i_L}$	$C = \frac{V_o \cdot (2D-1)}{(3-4D) \cdot f_s \cdot \Delta V_c \cdot R}$; $C_o = \frac{V_o \cdot D}{f_s \cdot \Delta V_o \cdot R}$	$L_1 = L_2 = 5\,\mu H$	$C_1 = C_2 = 0.25\,\mu F$ $C_o = 10\,\mu F$
2-IBC	$L = \frac{V_{in} \cdot D}{f_s \cdot \Delta i_L}$	$C_o = \frac{V_o \cdot D}{f_s \cdot \Delta V_o \cdot R}$	$L_1 = L_2 = 100\,\mu H$	$C_0 = 10\,\mu F$
4-IBC	$L = \frac{V_{in} \cdot D}{f_s \cdot \Delta i_L}$	$C_o = \frac{V_o \cdot D}{f_s \cdot \Delta V_o \cdot R}$	$L_1 = L_2 = L_3 = L_4 = 100\,\mu H$	$C_o = 10\,\mu F$
1st M-IBC	$L = \frac{V_{in} \cdot D}{f_s \cdot \Delta i_L}$	$C = \frac{V_o \cdot D}{f_s \cdot \Delta V_o}$; $C_o = \frac{V_o \cdot D}{f_s \cdot \Delta V_o \cdot R}$	$L_1 = L_2 = 100\,\mu H$	$C_x = 40{,}000\,\mu F$ $C_o = 10\,\mu F$

Table 1. *Cont.*

Converter Type	Equations		Parameters	
	Inductors	**Capacitors**	**Inductors**	**Capacitors**
2nd M-IBC	$L = \frac{V_{in} \cdot D}{f_s \cdot \Delta i_L}$	$C = \frac{V_o \cdot D}{f_s \cdot \Delta V_o}$; $C_o = \frac{V_o \cdot D}{f_s \cdot \Delta V_o \cdot R}$	$L_1 = L_2 = 100\,\mu H$	$C_1 = C_2 = 40{,}000\,\mu F$ $C_o = 10\,\mu F$
3rd M-IBC	$L_1 = \frac{V_{in} \cdot D}{f_s \cdot \Delta i_L}$; $L_2 = \frac{V_{in} \cdot D \cdot (2-D)}{f_s \cdot \Delta i_L}$	$C_1 = \frac{V_o \cdot D}{f_s \cdot \Delta V_c \cdot R \cdot (1-D)^2}$; $C_2 = \frac{V_o \cdot D}{f_s \cdot \Delta V_c \cdot R}$; $C_o = \frac{V_o \cdot D}{f_s \cdot \Delta V_o \cdot R}$	$L_1 = L_2 = 150\,\mu H$	$C_1 = C_2 = 4\,\mu F$ $C_o = 10\,\mu F$
PSOL	$L = \frac{V_{in} \cdot D}{f_s \cdot \Delta i_L}$	$C = \frac{V_o \cdot D}{f_s \cdot \Delta V_c \cdot R}$; $C_o = \frac{V_o \cdot D}{f_s \cdot \Delta V_o \cdot R}$	$L_1 = 100\,\mu H$	$C_1 = 5\,\mu F$ $C_o = 10\,\mu F$
1st M-PSOL	$L = \frac{V_{in} \cdot D}{f_s \cdot \Delta i_L}$	$C = \frac{V_o \cdot D}{f_s \cdot \Delta V_c \cdot R}$; $C_o = \frac{V_o \cdot D}{f_s \cdot \Delta V_o \cdot R}$	$L_1 = L_2 = 100\,\mu H$	$C_1 = 5\,\mu F$ $C_o = 10\,\mu F$
2nd M-PSOL	$L = \frac{V_{in} \cdot D}{f_s \cdot \Delta i_L}$	$C = \frac{V_o \cdot D}{f_s \cdot \Delta V_c \cdot R}$; $C_o = \frac{V_o \cdot D}{f_s \cdot \Delta V_o \cdot R}$	$L_1 = L_2 = 100\,\mu H$	$C_x = C_1 = 5\,\mu F$ $C_o = 10\,\mu F$
3rd M-PSOL	$L_1 = \frac{V_{in} \cdot D}{f_s \cdot \Delta i_L}$; $L_2 = \frac{V_{in} \cdot D}{f_s \cdot \Delta i_L \cdot (1-D)}$	$C_1 = \frac{V_o \cdot D}{f_s \cdot \Delta V_c \cdot R \cdot (1-D)}$; $C_2 = \frac{V_o \cdot D}{f_s \cdot \Delta V_c \cdot R}$; $C_o = \frac{V_o \cdot D}{f_s \cdot \Delta V_o \cdot R}$	$L_1 = L_2 = 130\,\mu H$	$C_1 = C_2 = 8\,\mu F$ $C_o = 10\,\mu F$
4th M-PSOL	$L_1 = \frac{V_{in} \cdot D}{f_s \cdot \Delta i_L}$; $L_2 = \frac{V_{in} \cdot D}{f_s \cdot \Delta i_L \cdot (1-D)}$	$C_1 = \frac{V_o \cdot D}{f_s \cdot \Delta V_c \cdot R \cdot (1-D)}$; $C_2 = \frac{V_o \cdot D}{f_s \cdot \Delta V_c \cdot R}$; $C_o = \frac{V_o \cdot D}{f_s \cdot \Delta V_o \cdot R}$	$L_1 = L_2 = 130\,\mu H$	$C_1 = C_2 = 8\,\mu F$ $C_o = 10\,\mu F$
SEPIC	$L = \frac{V_{in} \cdot D}{f_s \cdot \Delta i_L}$	$C = \frac{V_o \cdot D}{f_s \cdot \Delta V_c \cdot R}$; $C_o = \frac{V_o \cdot D}{f_s \cdot \Delta V_o \cdot R}$	$L_1 = L_2 = 100\,\mu H$	$C_1 = 4\,\mu F$ $C_o = 10\,\mu F$
1st M-SEPIC	$L = \frac{V_{in} \cdot D}{f_s \cdot \Delta i_L}$	$C = \frac{V_o \cdot D}{f_s \cdot \Delta V_c \cdot R}$; $C_o = \frac{V_o \cdot D}{f_s \cdot \Delta V_o \cdot R}$	$L_1 = L_2 = 100\,\mu H$	$C_1 = C_x = 4\,\mu F$ $C_o = 10\,\mu F$

Table 1. *Cont.*

Converter Type	Equations		Parameters	
	Inductors	**Capacitors**	**Inductors**	**Capacitors**
2nd M-SEPIC	$L = \frac{V_{in} \cdot D}{f_s \cdot \Delta i_L}$	$C = \frac{V_o \cdot D}{f_s \cdot \Delta V_c \cdot R}; C_o = \frac{V_o \cdot D}{f_s \cdot \Delta V_o \cdot R}$	$L_1 = L_2 = 100\,\mu H$	$C_1 = C_2 = C_3 = C_4 = 5\,\mu F$ $C_o = 10\,\mu F$
3rd M-SEPIC	$L = \frac{V_{in} \cdot D}{f_s \cdot \Delta i_L}$	$C = \frac{V_o \cdot D}{f_s \cdot \Delta V_c \cdot R}; C_o = \frac{V_o \cdot D}{f_s \cdot \Delta V_o \cdot R}$	$L_1 = L_2 = L_3 = 100\,\mu H$	$C_1 = C_2 = 5\,\mu F$ $C_o = 10\,\mu F$
4th M-SEPIC	$L = \frac{V_{in} \cdot D}{f_s \cdot \Delta i_L}$	$C = \frac{V_o \cdot D}{f_s \cdot \Delta V_c \cdot R}; C_o = \frac{V_o \cdot D}{f_s \cdot \Delta V_o \cdot R}$	$L_1 = L_2 = L_3 = 100\,\mu H$	$C_1 = C_2 = C_3 = C_4 = 5\,\mu F$ $C_o = 10\,\mu F$

4. Comparison Results

This study presents an analytical comparison between the most common non-isolated DC-DC converters. These converters are utilized in MATLAB/Simulink for comparison with several vital performances. Figure 26 displays the output voltage of converters when these converters operate at 0.5 duty cycle. The 1st M-TBC converter reaches 12 times the input voltage, which means this converter can be considered to exhibit the highest voltage gain compared with other converter types.The voltage gain ratio for each DC-DC converter studied in this paper are illustrated in Figure 27. The duty ratio range for applied comparison is between (0–0.8) to determine which converter has the highest voltage gain ratio. From Figure 27 mentioned above, the 1st M-TLBC converter can achieve a 50 voltage gain ratio when the duty cycle equals 0.74. Nevertheless, this voltage gain ratio can only be reached in the theoretical calculation, so these converters (1st M-TBC, 3rd M-IBC, 3rd M-PSOL, 4th M-PSOL, and 4th M-SEPIC) consider the highest voltage gain ratio that achieves 30 times. The voltage stress on the switch in these converters was calculated based on the duty range between (0–0.8), as depicted in Figure 28. The TLBC and 2nd M-TLBC appear to have less voltage stress values when compared with other converter types. The voltage stress equals 60 V at duty equals 0.8. Furthermore, the output voltage ripple is another essential factor that is considered for comparison between DC-DC converter types. Figure 29 illustrates the voltage ripple for each converter when these converters operate at 0.5 duty cycle. The ripple in the output voltage waveform of these (DBC, TBC,1ST M-TBC, 1st M-PSOL, and 2nd M-SEPIC) converters is more than 1 volt. Furthermore, the 1st M-TBC can be classified as including the highest converter ripple in output voltage equal to 5 volts. Other converters not mentioned are less than 1-volt ripple in output voltage, so in this state, all the converters produce a good performance.

Table 2 lists a summary of the converters utilized in this study; the considered typical parameters are the equation for calculating voltage gain, the equation for calculating voltage stress on the switch, and these converters consist of the number of components. The converters (PSOL and SEPIC) appear as fewer components required, while the converters (1st M-TBC and 4th M-PSOL) appear as higher components. The number of components is essential for comparing these converters depending on the size and ease of implementation of critical performance parameter comparison. When comparing the converters, they are classified into three categories suitable for low-voltage applications, medium-voltage applications, and high-voltage applications to appear in which field this converter is appropriate. For lower voltage applications, these converters (DBC, DuBC, TLBC, 2-IBC, 1st M-IBC, PSOL, SEPIC, and 1st M-SEPIC) are suitable and reasonable because of the lower cost, smaller size, and have less switch stress. While the converters (TBC, 1st M-TLBC, 2nd M-TLBC, 4-IBC, 1st M-IBC, 2nd M-IBC, 1st M-PSOL, 2nd M-PSOL, 1st M-SEPIC, and 2nd M-SEPIC) are more efficient and suitable for medium-voltage applications. The high-voltage applications require converters with high-voltage gain but without increasing cost and more difficult implementation of the converter circuit. So, the converters (TBC, 1st M-TBC, 2nd M-IBC, 3rd M-IBC, 3rd M-PSOL, 4th M-PSOL, 2nd M-SEPIC, 3rd M-SEPIC, and 4th M-SEPIC) are more appropriate for high-voltage applications. Figure 30 illustrates the result of the comparisons relative to the different performance factors for comprehensively clarifying these converters in which categories are sufficient and proper should be utilized. Numbers from 1 to 10 are used to assess the different topologies. Number 1 expresses the worst performance, whereas 10 denotes the best performance.

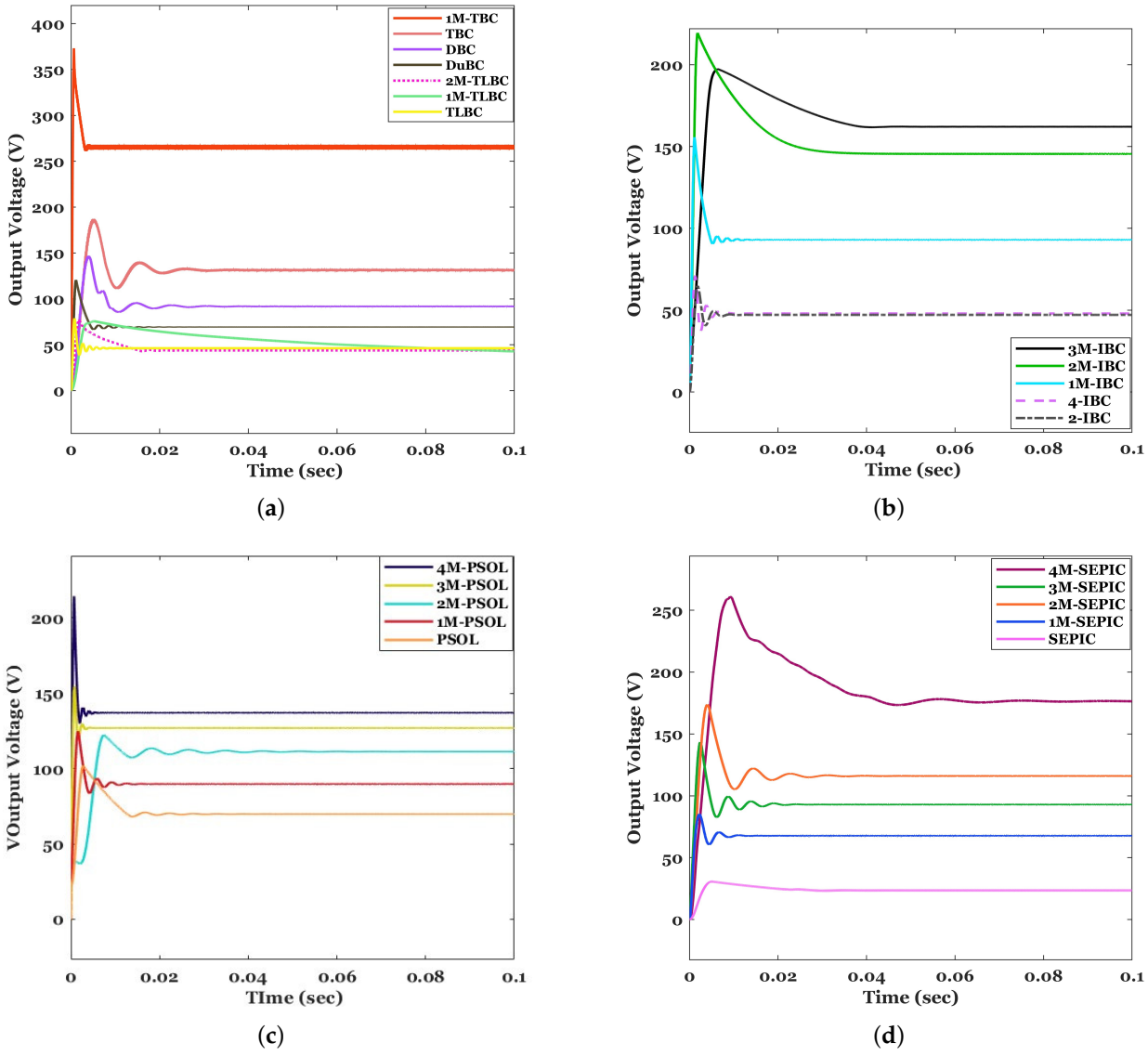

Figure 26. Output Voltage of Converters at $D = 0.5$ (**a**) Group 1 (DBC, TBC, 1st M-TBC, DuBC, TLBC, 1st M-TLBC, and 2nd M-TLBC) (**b**) Group 2 (2-IBC, 4-IBC, 1st M-IBC, 2nd M-IBC, and 3rd M-IBC) (**c**) Group 3 (PSOL, 1st M-PSOL, 2nd M-PSOL, 3rd M-PSOL, and 4th M-PSOL) (**d**) Group 4 (SEPIC, 1st M-SEPIC, 2nd M-SEPIC, 3rd M-SEPIC, and 4th M-SEPIC).

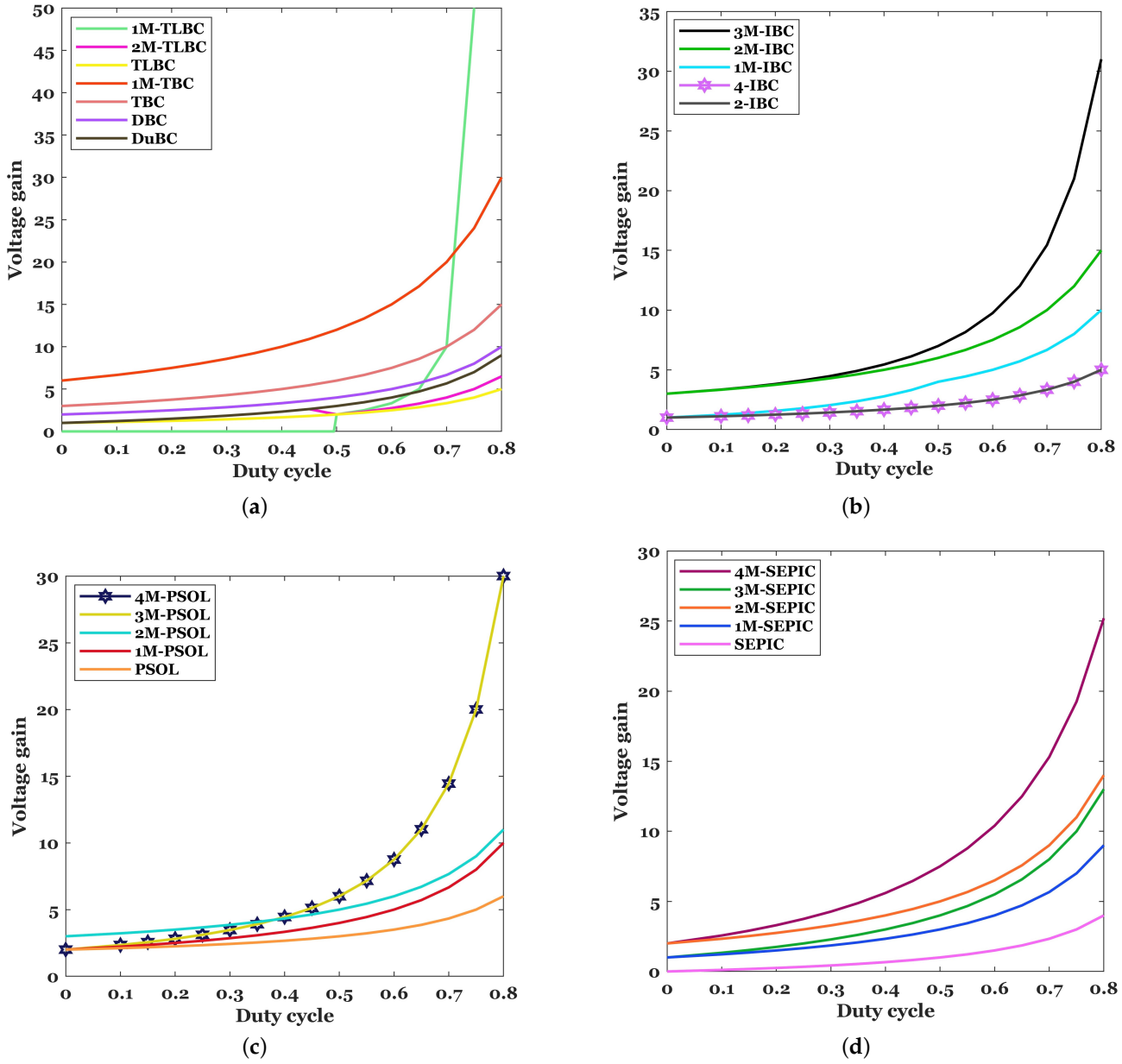

Figure 27. Voltage Gain ratio of Converters (**a**) Group 1 (DBC, TBC, 1st M-TBC, DuBC, TLBC, 1st M-TLBC, and 2nd M-TLBC) (**b**) Group 2 (2-IBC, 4-IBC, 1st M-IBC, 2nd M-IBC, and 3rd M-IBC) (**c**) Group 3 (PSOL, 1st M-PSOL, 2nd M-PSOL, 3rd M-PSOL, and 4th M-PSOL) (**d**) Group 4 (SEPIC, 1st M-SEPIC, 2nd M-SEPIC, 3rd M-SEPIC, and 4th M-SEPIC).

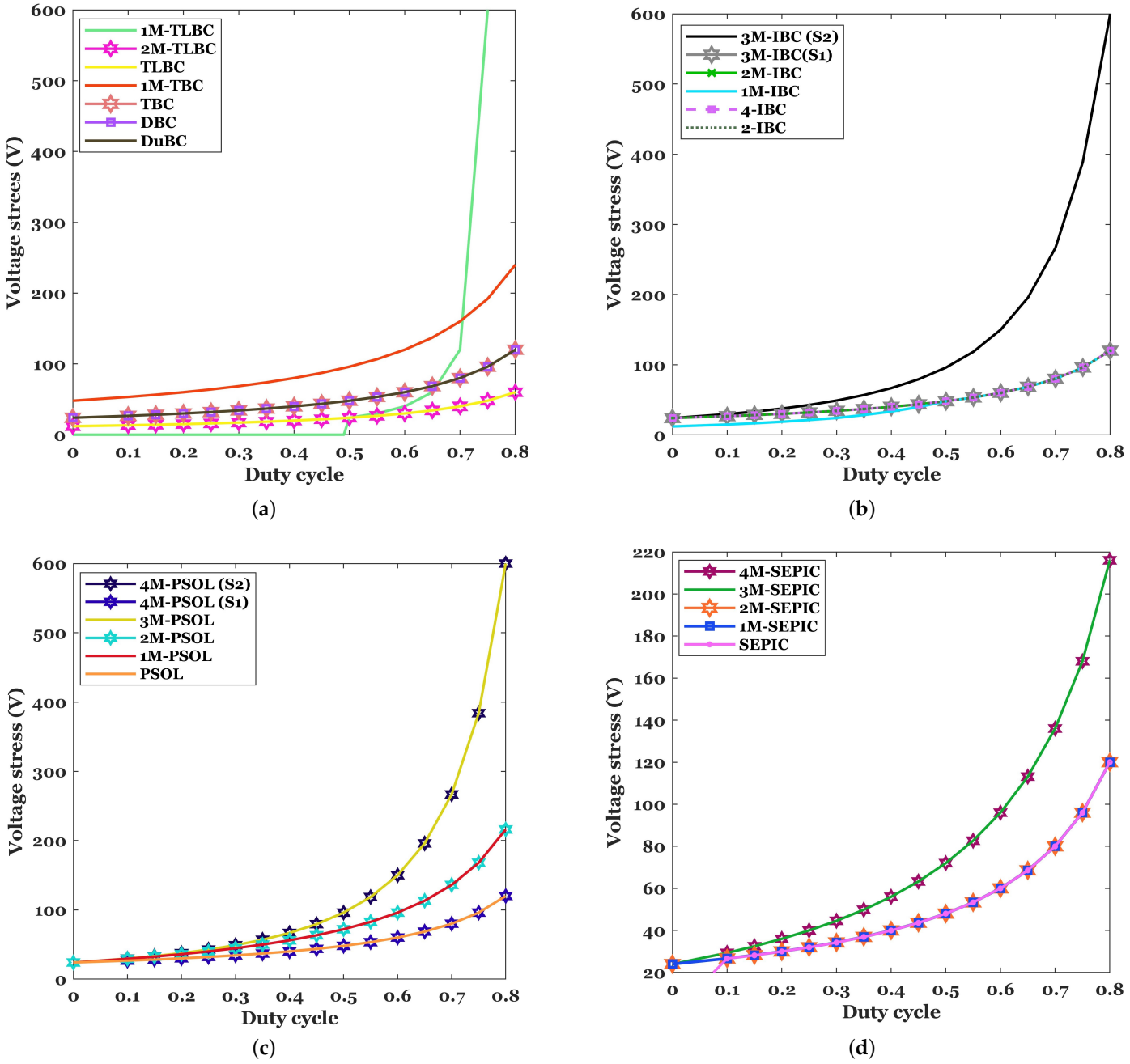

Figure 28. Voltage Stress on Switch *S* of Converters (**a**) Group 1 (DBC, TBC, 1st M-TBC, DuBC, TLBC, 1st M-TLBC, and 2nd M-TLBC) (**b**) Group 2 (2-IBC, 4-IBC, 1st M-IBC, 2nd M-IBC, and 3rd M-IBC) (**c**) Group 3 (PSOL, 1st M-PSOL, 2nd M-PSOL, 3rd M-PSOL, and 4th M-PSOL) (**d**) Group 4 (SEPIC, 1st M-SEPIC, 2nd M-SEPIC, 3rd M-SEPIC, and 4th M-SEPIC).

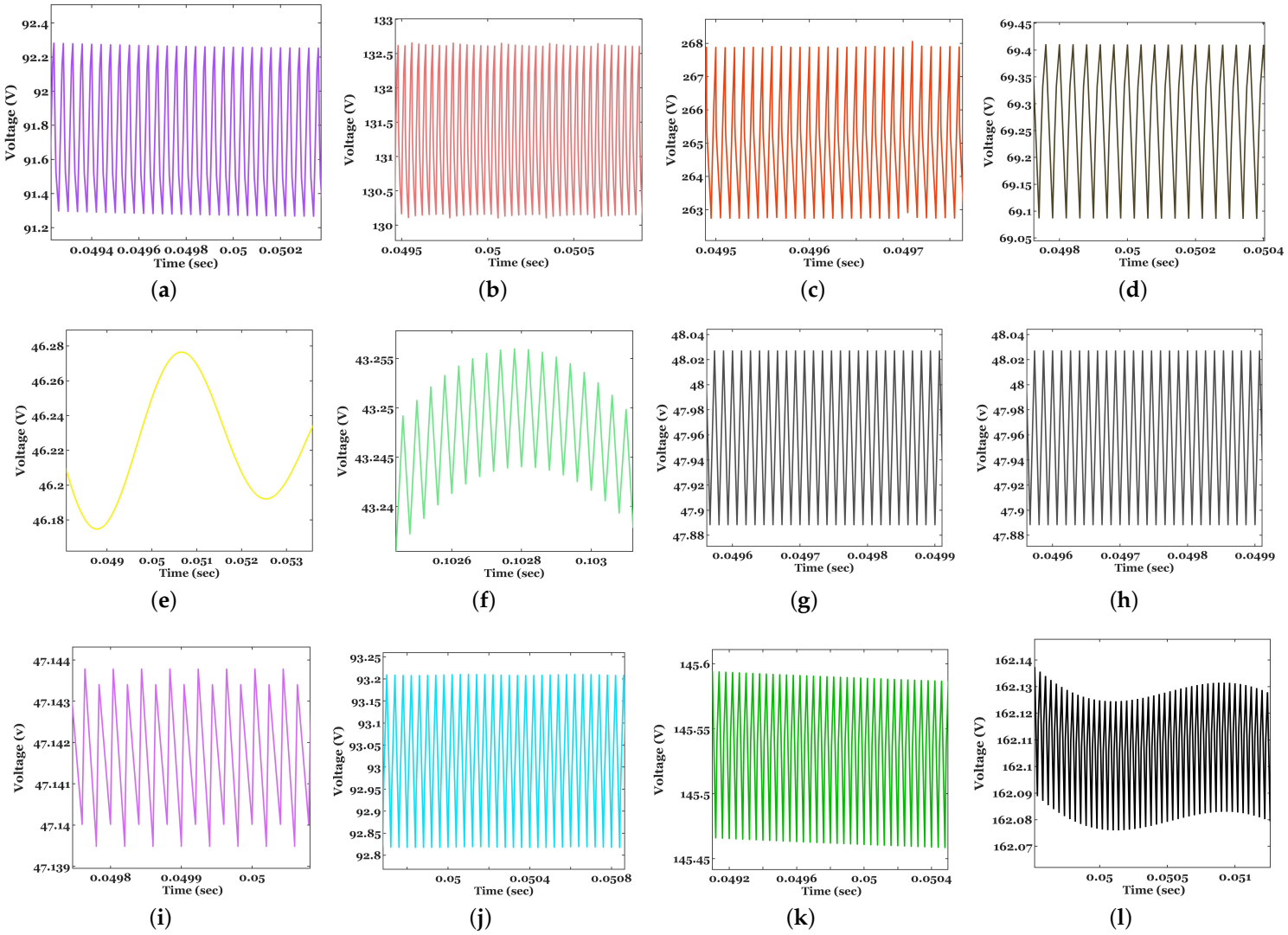

Figure 29. *Cont.*

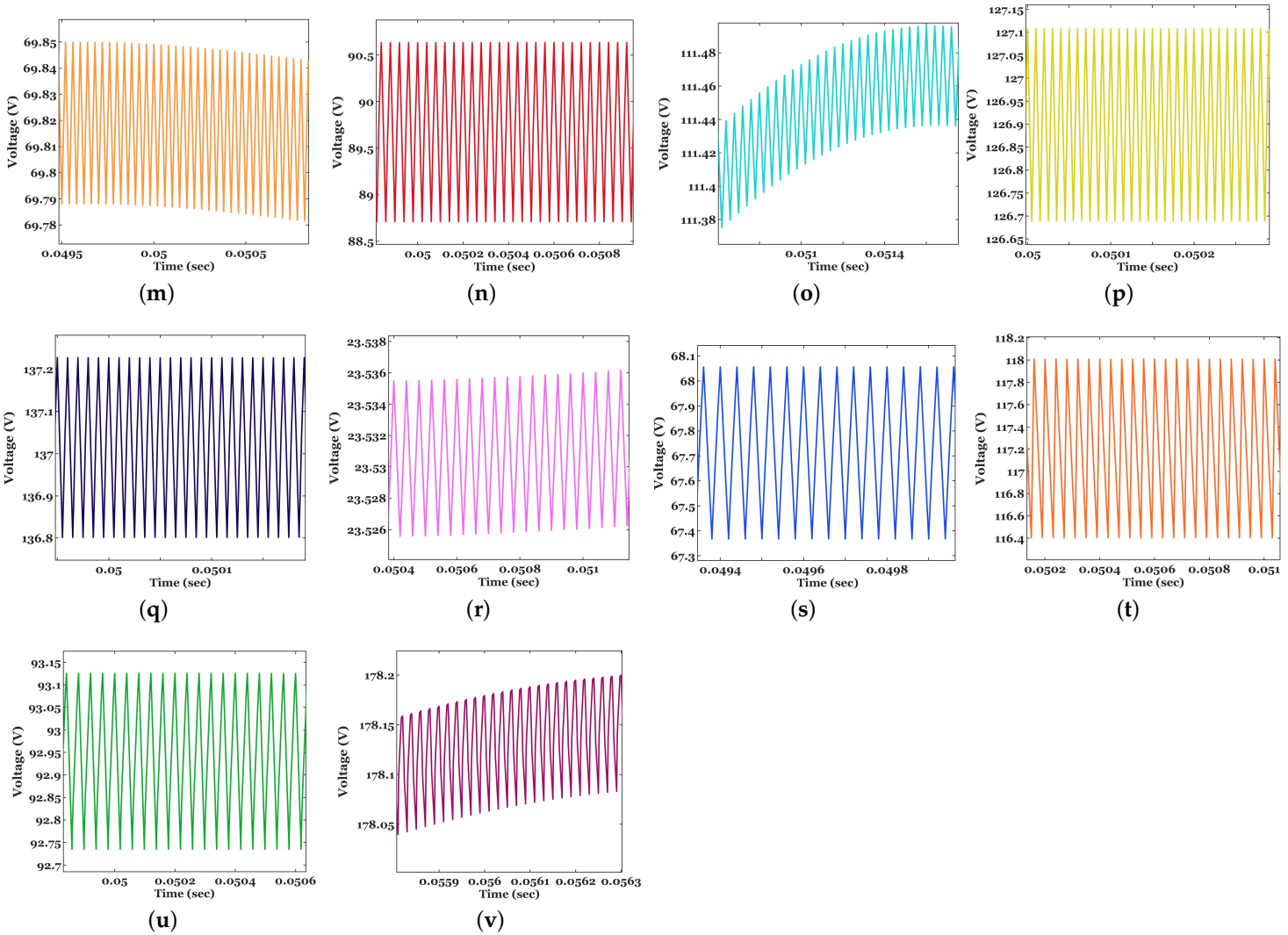

Figure 29. Voltage Ripple (**a**) DBC (**b**) TBC (**c**) 1st M-TBC (**d**) DuBC (**e**) TLBC (**f**) 1st M-TLBC (**g**) 2nd M-TLBC (**h**) 2-IBC (**i**) 4-IBC (**j**) 1st M-IBC (**k**) 2nd M-IBC (**l**) 3rd M-IBC (**m**) PSOL (**n**) 1st M-PSOL (**o**) 2nd M-PSOL (**p**) 3rd M-PSOL (**q**) 4th M-PSOL (**r**) SEPIC (**s**) 1st M-SEPIC (**t**) 2nd M-SEPIC (**u**) 3rd M-SEPIC (**v**) 4th M-SEPIC.

Table 2. Summary of converter characteristics.

Converter Type	No. of Components				Voltage Gain	Voltage Stress Across the Switch S
	S	L	C	D		
DBC	1	1	3	3	$\frac{2}{1-D}$	$\frac{V_o}{2}$
TBC	1	1	5	5	$\frac{3}{1-D}$	$\frac{V_o}{3}$
1st M-TBC	1	2	6	7	$\frac{6}{1-D}$	$\frac{V_o}{3}$
DuBC	2	2	1	3	$\frac{1+D}{1-D}$	$\frac{V_o+V_{in}}{2}$
TLBC	2	1	2	2	$\frac{1}{1-D}$	$\frac{V_o}{2}$
1st M-TLBC	2	2	4	3	$\frac{2}{3-4\cdot D}$	$\frac{V_o}{2}$
2nd M-TLBC	2	2	4	3	$\begin{cases} \frac{1+D}{1-D} & D < 0.5 \\ \frac{0.5+D}{1-D} & D \geq 0.5 \end{cases}$	$\begin{cases} \frac{V_o}{2(1+D)} & D < 0.5 \\ \frac{V_o}{1+2D} & D \geq 0.5 \end{cases}$
2-IBC	2	2	1	2	$\frac{1}{1-D}$	V_o
4-IBC	4	4	1	4	$\frac{1}{1-D}$	V_o
1st M-IBC	2	2	2	2	$\begin{cases} \frac{1}{(1-D)^2} & D < 0.5 \\ \frac{2}{1-D} & D \geq 0.5 \end{cases}$	$\frac{V_o}{2}$
2nd M-IBC	2	2	3	3	$\frac{3}{1-D}$	$\frac{V_o}{3}$
3rd M-IBC	2	2	3	3	$\frac{3-3\cdot D+D^2}{(1-D)^2}$	$V_{S1} = \frac{V_o\cdot(1-D)}{3-3\cdot D+D^2}$; $V_{S2} = \frac{V_o}{3-3\cdot D+D^2}$
PSOL	1	1	2	2	$\frac{2-D}{1-D}$	$\frac{V_o}{2-D}$
1st M-PSOL	1	2	2	5	$\frac{2}{1-D}$	$\frac{V_{in}\cdot(1+D)}{1-D}$
2nd M-PSOL	1	2	3	4	$\frac{3-D}{1-D}$	$\frac{V_{in}\cdot(1+D)}{1-D}$
3rd M-PSOL	1	2	3	4	$\frac{2-D}{(1-D)^2}$	$\frac{V_{in}}{(1-D)^2}$
4th M-PSOL	2	2	3	3	$\frac{2-D}{(1-D)^2}$	$V_{S1} = \frac{V_{in}}{1-D}$; $V_{S2} = \frac{V_{in}}{(1-D)^2}$
SEPIC	1	2	2	1	$\frac{D}{1-D}$	$\frac{V_o}{D}$
1st M-SEPIC	1	2	3	2	$\frac{1+D}{1-D}$	$\frac{V_{in}}{1-D}$
2nd M-SEPIC	1	2	4	4	$\frac{2+D}{1-D}$	$\frac{V_{in}}{1-D}$
3rd M-SEPIC	1	3	3	5	$\frac{1+2\cdot D}{1-D}$	$\frac{V_{in}\cdot(1+D)}{1-D}$
4th M-SEPIC	1	3	5	7	$\frac{2+3\cdot D+D^2}{1-D}$	$\frac{V_o}{2+D}$

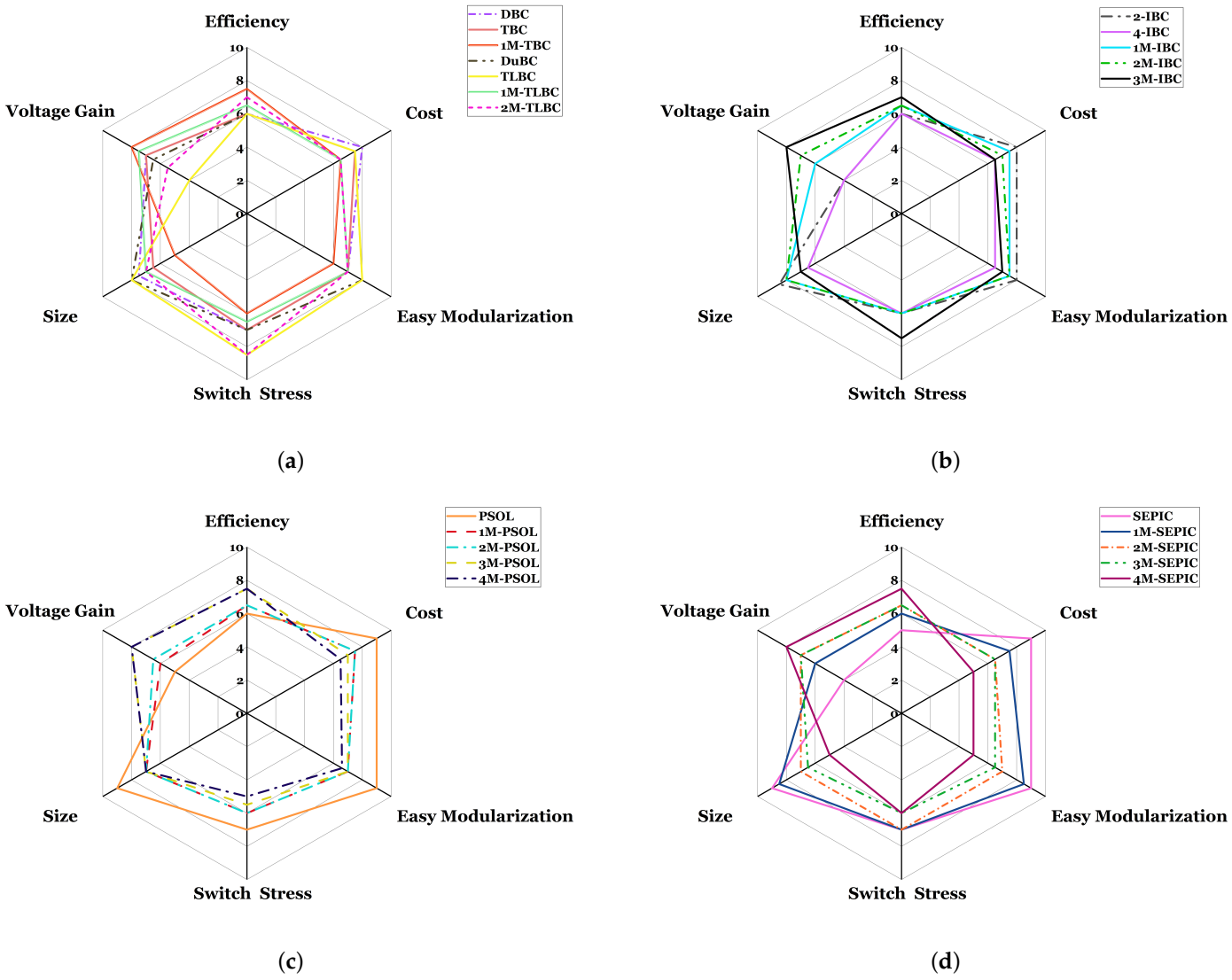

Figure 30. Radar Chart for Summarize Comparison (**a**) Group 1 (DBC, TBC, 1st M-TBC, DuBC, TLBC, 1st M-TLBC, and 2nd M-TLBC) (**b**) Group 2 (2-IBC, 4-IBC, 1st M-IBC, 2nd M-IBC, and 3rd M-IBC) (**c**) Group 3 (PSOL, 1st M-PSOL, 2nd M-PSOL, 3rd M-PSOL, and 4th M-PSOL) (**d**) Group 4 (SEPIC, 1st M-SEPIC, 2nd M-SEPIC, 3rd M-SEPIC, and 4th M-SEPIC).

5. Conclusions

The performances of several non-isolated DC-DC converter topologies were comprehensively investigated to assess which converter is more suitable for FC applications. Based on the voltage gain, voltage stress, size of the circuit, and efficiency, the DC-DC converters were broadly classified depending on voltage-level applications, which are categorized into three groups: low-level voltage, medium-level voltage, and high-level voltage. Based on the comparison results, low-voltage applications are best served by converters such as DBC, DuBC, TLBC, 2-IBC, 1st M-IBC, PSOL, SEPIC, and 1st M-SEPIC due to their lower cost, smaller size, and reduced switch stress. Medium-voltage applications are best suited to converters such as TBC, 1st M-TLBC, 2nd M-TLBC, 4-IBC, 1st M-IBC, 2nd M-IBC, 1st M-PSOL, 2nd M-PSOL, 1st M-SEPIC, and 2nd M-SEPIC, which offer higher efficiency. Finally, high-voltage applications are best served by converters such as TBC, 1st M-TBC, 2nd M-IBC, 3rd M-IBC, 3rd M-PSOL, 4th M-PSOL, 2nd M-SEPIC, 3rd M-SEPIC, and 4th M-SEPIC.

Author Contributions: Conceptualization, F.A.A. and T.A.A.-J.; methodology, F.A.A. and T.A.A.-J.; software, F.A.A. and T.A.A.-J.; validation, F.A.A., T.A.A.-J. and A.A.O.; formal analysis, F.A.A. and T.A.A.; investigation, F.A.A. and T.A.A.; resources, F.A.A.,T.A.A.-J., A.A.O. and A.K.; data curation, F.A.A. and T.A.A.-J.; writing—original draft preparation, F.A.A.,T.A.A.-J., A.A.O. and A.K.; writing—review and editing, F.A.A.,T.A.A.-J., A.A.O., A.K. and M.K.; visualization, F.A.A., T.A.A.-J. and A.K.; supervision, A.A.O., A.K. and M.K.; project administration, T.A.A.-J., A.K., M.K. and T.W.; funding acquisition, A.K., M.K. and T.W. All authors have read and agreed to the published version of the manuscript.

Funding: This research is funded by MORE/ELAPSED as part of dtec.bw—Digitalization and Technology Research Center of the Bundeswehr which we gratefully acknowledge.

Conflicts of Interest: The authors declare no conflict of interest.

Abbreviations

The following abbreviations are used in this manuscript:

DuBC	Double-boost converter
D	Duty Cycle
FC	Fuel Cell
GHG	Greenhouse Gas
IBC	Interleaved Boost Converter
MLBC	Multilevel Boost Converter
PV	Photovoltaic
PSOL	Positive Output Super Lift
PEMFC	Proton Exchange Membrane Fuel Cell
RES	Renewable Energy Source
SEPIC	Single-Ended Primary Inductor Converter
TLBC	Three-level boost converter

References

1. Taghvaee, M.H.; Radzi, M.A.M.; Moosavain, S.M.; Hizam, H.; Hamiruce Marhaban, M. A current and future study on non-isolated DC–DC converters for photovoltaic applications. *Renew. Sustain. Energy Rev.* **2013**, *17*, 216–227. [CrossRef]
2. Li, W.; He, X. Review of Nonisolated High-Step-Up DC/DC Converters in Photovoltaic Grid-Connected Applications. *IEEE Trans. Ind. Electron.* **2011**, *58*, 1239–1250. [CrossRef]
3. Buberger, J.; Kersten, A.; Kuder, M.; Eckerle, R.; Weyh, T.; Thiringer, T. Total CO_2-equivalent life-cycle emissions from commercially available passenger cars. *Renew. Sustain. Energy Rev.* **2022**, *159*, 112158. [CrossRef]
4. Oliveira, A.M.; Beswick, R.R.; Yan, Y. A green hydrogen economy for a renewable energy society. *Curr. Opin. Chem. Eng.* **2021**, *33*, 100701. [CrossRef]
5. Karami, N.; Outbib, R.; Moubayed, N. Fuel flow control of a PEM Fuel Cell with MPPT. In Proceedings of the International Symposium on Intelligent Control, Dubrovnik, Croatia, 3–5 October 2012; pp. 289–294. [CrossRef]
6. Khan, F.; Nawaz, A.; Muhammad, M.; Ali, M. Review and Analysis of MATLAB® Simulink Model Of PEM Fuel Cell Stack. *Int. J. Eng. Comput. Sci.* **2013**, *13*, 31–34 .
7. Sivakumar, S.; Sathik, M.J.; Manoj, P.S.; Sundararajan, G. An assessment on performance of DC–DC converters for renewable energy applications. *Renew. Sustain. Energy Rev.* **2016**, *58*, 1475–1485. [CrossRef]
8. Kolli, A.; Gaillard, A.; De Bernardinis, A.; Bethoux, O.; Hissel, D.; Khatir, Z. A review on DC/DC converter architectures for power fuel cell applications. *Energy Convers. Manag.* **2015**, *105*, 716–730. [CrossRef]
9. Mumtaz, F.; Zaihar Yahaya, N.; Tanzim Meraj, S.; Singh, B.; Kannan, R.; Ibrahim, O. Review on non-isolated DC-DC converters and their control techniques for renewable energy applications. *Ain Shams Eng. J.* **2021**, *12*, 3747–3763. [CrossRef]
10. Arunkumari, T.; Indragandhi, V. An overview of high voltage conversion ratio DC-DC converter configurations used in DC micro-grid architectures. *Renew. Sustain. Energy Rev.* **2017**, *77*, 670–687. [CrossRef]
11. Lai, J.S. Power conditioning circuit topologies. *IEEE Ind. Electron. Mag.* **2009**, *3*, 24–34. [CrossRef]
12. Rosas-Caro, J.C.; Ramirez, J.M.; Garcia-Vite, P.M. Novel DC-DC Multilevel Boost Converter. In Proceedings of the Power Electronics Specialists Conference, Rhodes, Greece, 15–19 June 2008; pp. 2146–2151. [CrossRef]
13. Rosas-Caro, J.; Ramirez, J.; Peng, F.; Valderrabano, A. A DC–DC multilevel boost converter. *IET Power Electron.* **2010**, *3*, 129–137. [CrossRef]
14. İNcİ, M. Design and Analysis of Dual Level Boost Converter Based Transformerless Grid Connected PV System for Residential Applications. In Proceedings of the 4th International Conference on Power Electronics and their Applications (ICPEA), Elazig, Turkey, 25–27 September 2019; pp. 1–6. [CrossRef]

15. Alsafrani, A.; Parker, M.; Shahbazi, M.; Horsfall, A. High Gain DC-DC Multilevel Boost Converter to Enable Transformerless Grid Connection for Renewable Energy. In Proceedings of the 56th International Universities Power Engineering Conference (UPEC), Middlesbrough, UK, 31 August–3 September 2021; pp. 1–6. [CrossRef]
16. Alsafrani, A.; Shahbazi, M.; Horsfall, A. High gain DC-DC voltage lift switched-inductor multilevel boost converter for supporting grid connection of wave energy conversion. In Proceedings of the 11th International Conference on Power Electronics, Machines and Drives (PEMD 2022), Hybrid Conference, Newcastle, UK, 21–23 June 2022; pp. 754–758. [CrossRef]
17. Youn, H.S.; Yun, D.H.; Lee, W.S.; Lee, I.O. Study on Boost Converters with High Power-Density for Hydrogen-Fuel-Cell Hybrid Railway System. *Electronics* **2020**, *9*, 771. [CrossRef]
18. Zhang, Y.; Shi, J.; Zhou, L.; Li, J.; Sumner, M.; Wang, P.; Xia, C. Wide Input-Voltage Range Boost Three-Level DC–DC Converter With Quasi-Z Source for Fuel Cell Vehicles. *IEEE Trans. Power Electron.* **2017**, *32*, 6728–6738. [CrossRef]
19. Elsayad, N.; Moradisizkoohi, H.; Mohammed, O.A. A Three-Level Boost Converter with an Extended Gain and Reduced Voltage Stress using WBG Devices. In Proceedings of the 6th Workshop on Wide Bandgap Power Devices and Applications (WiPDA), Atlanta, GA, USA, 31 October–2 November 2018; pp. 45–50. [CrossRef]
20. Nahar, S.; Uddin, M.B. Analysis the performance of interleaved boost converter. In Proceedings of the 4th International Conference on Electrical Engineering and Information & Communication Technology (iCEEiCT), Dhaka, Bangladesh, 13–15 September 2018; pp. 547–551. [CrossRef]
21. Harinee, M.; Nagarajan, V.S.; Dimple; Seyezhai, R.; Mathur, B.L. Modeling and design of fuel cell based two phase interleaved boost converter. In Proceedings of the 1st International Conference on Electrical Energy Systems, Chennai, India, 3–5 January 2011; pp. 72–77. [CrossRef]
22. Chen, C.; Wang, C.; Hong, F. Research of an interleaved boost converter with four interleaved boost convert cells. In Proceedings of the Asia Pacific Conference on Postgraduate Research in Microelectronics & Electronics (PrimeAsia), Shanghai, China, 19–21 January 2009; pp. 396–399. [CrossRef]
23. Jang, Y.; Jovanovic, M.M. Interleaved Boost Converter With Intrinsic Voltage-Doubler Characteristic for Universal-Line PFC Front End. *IEEE Trans. Power Electron.* **2007**, *22*, 1394–1401. [CrossRef]
24. Zhou, L.W.; Zhu, B.X.; Luo, Q.M.; Chen, S. Interleaved non-isolated high step-up DC/DC converter based on the diode–capacitor multiplier. *IET Power Electron.* **2014**, *7*, 390–397. [CrossRef]
25. Varesi, K.; Hassanpour, N.; Saeidabadi, S. Novel high step-up DC–DC converter with increased voltage gain per devices and continuous input current suitable for DC microgrid applications. *Int. J. Circuit Theory Appl.* **2020**, *48*, 1820–1837. [CrossRef]
26. Fang Lin, L.; Hong, Y. Positive output super-lift converters. *IEEE Trans. Power Electron.* **2003**, *18*, 105–113. [CrossRef]
27. Berkovich, Y.; Axelrod, B.; Madar, R.; Twina, A. Improved Luo converter modifications with increasing voltage ratio. *IET Power Electron.* **2015**, *8*, 202–212. [CrossRef]
28. Mohammed, A.T.; Alshamaa, N.K. Design and Implementation of a Modified Luo Converter with Higher–Voltage Ratio Gain. *IOP Conf. Ser. Mater. Sci. Eng.* **2020**, *881*, 012124. [CrossRef]
29. Gholizadeh, H.; Sharifi Shahrivar, R.; Hashemi, M.R.; Afjei, E.; A. Gorji, S. Design and Implementation a Single-Switch Step-Up DC-DC Converter Based on Cascaded Boost and Luo Converters. *Energies* **2021**, *14*, 3584. [CrossRef]
30. Mahdizadeh, S.; Gholizadeh, H.; Gorji, S.A. A Power Converter Based on the Combination of Cuk and Positive Output Super Lift Lou Converters: Circuit Analysis, Simulation and Experimental Validation. *IEEE Access* **2022**, *10*, 52899–52911. [CrossRef]
31. Verma, M.; Kumar, S.S. Hardware Design of SEPIC Converter and its Analysis. In Proceedings of the International Conference on Current Trends towards Converging Technologies (ICCTCT), Coimbatore, India, 1–3 March 2018; pp. 1–4. [CrossRef]
32. Gu, W.; Zhang, D. *Designing a SEPIC Converter*; National Semiconductor Application Note 1484; National Semiconductor Corporation: Santa Clara, CA, USA, 2008.
33. Gules, R.; Santos, W.M.d.; Reis, F.A.d.; Romaneli, E.F.R.; Badin, A.A. A Modified SEPIC Converter With High Static Gain for Renewable Applications. *IEEE Trans. Power Electron.* **2014**, *29*, 5860–5871. [CrossRef]
34. Ozsoy, E.; Padmanaban, S.; Blaabjerg, F.; Ionel, D.M.; Kalla, U.K.; Bhaskar, M.S. Control of High Gain Modified SEPIC Converter: A Constant Switching Frequency Modulation Sliding Mode Controlling Technique. In Proceedings of the International Power Electronics and Application Conference and Exposition (PEAC), Shenzhen, China, 4–7 November 2018; IEEE: Piscataway, NJ, USA; pp. 1–6. [CrossRef]
35. Kumar, D.; Gupta, R.A.; Tiwari, H. A Novel High Voltage Gain SEPIC Converter Based on Hybrid Split-Inductor for Renewable Application. *IETE J. Res.* **2022**, *68*, 3457–3473. [CrossRef]
36. Ahmed, I.; Kahawish, T. Design and Implementation of High Gain SEPIC Converter. In Proceedings of the International Conference on Advanced Computer Applications (ACA), Maysan, Iraq, 25–26 July 2021; pp. 116–121. [CrossRef]
37. Ahmed, O.A.; Bleijs, J.A.M. An overview of DC–DC converter topologies for fuel cell-ultracapacitor hybrid distribution system. *Renew. Sustain. Energy Rev.* **2015**, *42*, 609–626. [CrossRef]
38. Pukrushpan, J.T.; Stefanopoulou, A.G.; Peng, H. *Control of Fuel Cell Power Systems: Principles, Modeling, Analysis and Feedback Design*, 1st ed.; Springer: London, UK, 2004. [CrossRef]
39. Fawzi, M.; El-Fergany, A.A.; Hasanien, H.M. Effective methodology based on neural network optimizer for extracting model parameters of PEM fuel cells. *Int. J. Energy Res.* **2019**, *43*, 8136–8147. [CrossRef]

40. Thounthong, P.; Rael, S.; Davat, B. Utilizing fuel cell and supercapacitors for automotive hybrid electrical system. In Proceedings of the 20th Annual Applied Power Electronics Conference and Exposition, Austin, TX, USA, 6–10 March 2005; pp. 90–96. [CrossRef]
41. Jeremy, L.J.; Ooi, C.A.; Teh, J. Non-isolated conventional DC-DC converter comparison for a photovoltaic system: A review. *J. Renew. Sustain. Energy* **2020**, *12*, 013502. [CrossRef]
42. Kersten, A.; Rodionov, A.; Kuder, M.; Hammarström, T.; Lesnicar, A.; Thiringer, T. Review of Technical Design and Safety Requirements for Vehicle Chargers and Their Infrastructure According to National Swedish and Harmonized European Standards. *Energies* **2021**, *14*, 3301. [CrossRef]
43. Wang, H.; Gaillard, A.; Hissel, D. A review of DC/DC converter-based electrochemical impedance spectroscopy for fuel cell electric vehicles. *Renew. Energy* **2019**, *141*, 124–138. [CrossRef]
44. Raghavendra, K.V.G.; Zeb, K.; Muthusamy, A.; Krishna, T.N.V.; Kumar, S.V.S.V.P.; Kim, D.H.; Kim, M.S.; Cho, H.G.; Kim, H.J. A Comprehensive Review of DC–DC Converter Topologies and Modulation Strategies with Recent Advances in Solar Photovoltaic Systems. *Electronics* **2020**, *9*, 31. [CrossRef]
45. Liu, Z.; Du, J.; Yu, B. Design Method of Double-Boost DC/DC Converter with High Voltage Gain for Electric Vehicles. *World Electr. Veh. J.* **2020**, *11*, 64. [CrossRef]
46. Hwu, K.I.; Yau, Y.T. An Interleaved AC–DC Converter Based on Current Tracking. *IEEE Trans. Ind. Electron.* **2009**, *56*, 1456–1463. [CrossRef]
47. Tomaszuk, A.; Krupa, A. High efficiency high step-up DC/DC converters—A review. *Bull. Pol. Acad. Sci. Tech. Sci.* **2011**, *59*, 475–483. [CrossRef]
48. Ramasamy, S.; Abishri, P.; Umashankar, S. Review of coupled two and three phase interleaved boost converter (IBC) and investigation of four phase IBC for renewable application. *Int. J. Renew. Energy Res.* **2016**, *6*, 421–434. [CrossRef]